SUPERHARMONIC INJECTION LOCKED QUADRATURE LC VCO USING CURRENT RECYCLING ARCHITECTURE

A Thesis

by

SHRIRAM KALUSALINGAM

Submitted to the Office of Graduate Studies of
Texas A&M University
in partial fulfillment of the requirements for the degree of

MASTER OF SCIENCE

December 2010

Major Subject: Electrical Engineering

SUPERHARMONIC INJECTION LOCKED QUADRATURE LC VCO USING CURRENT RECYCLING ARCHITECTURE

A Thesis

by

SHRIRAM KALUSALINGAM

Submitted to the Office of Graduate Studies of
Texas A&M University
in partial fulfillment of the requirements for the degree of

MASTER OF SCIENCE

Approved by:

Chair of Committee,	Aydin Ilker Karsilayan
Committee Members,	Jose Silva Martinez
	Peng Li
	Duncan Henry Walker
Head of Department,	Costas Georghiades

December 2010

Major Subject: Electrical Engineering

ABSTRACT

Superharmonic Injection Locked Quadrature LC VCO Using

Current Recycling Architecture. (December 2010)

Shriram Kalusalingam, B.E., Anna University

Chair of Advisory Committee: Dr. Aydin Ilker Karsilayan

Quadrature LO signal is a key element in many of the RF transceivers which tend to dominate today's wireless communication technology. The design of a quadrature LC VCO with better phase noise and lower power consumption forms the core of this work. This thesis investigates a coupling mechanism to implement a quadrature voltage controlled oscillator using indirect injection method. The coupling network in this QVCO couples the two LC cores with their super-harmonic and it recycles its bias current back into the LC tank such that the power consumed by the coupling network is insignificant. This recycled current enables the oscillator to achieve higher amplitude of oscillation for the same power consumption compared to conventional design, hence assuring better phase noise. Mathematical analysis has been done to study the mechanism of quadrature operation and mismatch effects of devices on the quadrature phase error of the proposed QVCO.

The proposed quadrature LC VCO is designed in TSMC 0.18 μm technology. It is tunable from 2.61 GHz - 2.85 GHz with sensitivity of 240 MHz/V. Its worst case phase

noise is -120 dBc/Hz at 1 MHz offset. The total layout area is 1.41 mm^2 and the QVCO core totally draws 3 mA current from 1.8 V supply.

To my parents and my brother

ACKNOWLEDGEMENTS

I would like to express my sincere gratitude to my advisor, my committee members, my colleagues, my friends, my parents and my brother. Without their support, the completion of this thesis would not have been possible.

I gratefully acknowledge my advisor, Dr. Aydin Karsilayan, for his guidance and encouragement throughout this research. He also provided a strong basis and great suggestions for my knowledge in the field of analog circuit design. He was always accessible and willing to help me.

I would like to thank Dr. Jose Silva-Martinez and Dr. Edgar Sanchez-Sinencio for what I learnt in their courses. I thank them for teaching me the most basic Analog and RF circuit design techniques.

I would like to express my gratitude to Jianhong Xiao (my mentor) and James Y. C. Chang (my manager) when I was doing my internship at Broadcom Corporation. In spite of busy schedules, Jianhong Xiao always had time to listen to me patiently and clarify all my doubts regarding circuit design.

TABLE OF CONTENTS

CHAPTER		Page
I	INTRODUCTION……..…….	1
	A. Goal of the research……..	2
	B. Thesis guide……..	2
II	BACKGROUND…….....	3
III	PROPOSED QUADRATURE VOLTAGE CONTROLLED OSCILLATOR……...……..	8
	A. Mechanism of quadrature operation…….……	15
	B. Quadrature inaccuracy due to mismatches…...……	19
	C. Phase noise analysis…….	28
IV	DESIGN OF QUADRATURE VOLTAGE CONTROLLED OSCILLATOR…….	33
	A. MOS varactor…….……..	34
	B. Center-tapped inductor……..…...	36
	C. Cross-coupled transistors……..……	38
V	POST LAYOUT SIMULATION RESULTS……...……	42
VI	CONCLUSION……...…….	49
REFERENCES……...……...		50
APPENDIX……...		53
VITA……...…….....		61

LIST OF FIGURES

FIGURE		Page
2.1	RC-CR circuit for quadrature generation……	3
2.2	Parallel coupled quadrature VCO (PQVCO)……...	5
2.3	Series coupled quadrature VCO (SQVCO)…….....	6
2.4	Quadrature VCO using superharmonic coupling……..…..	7
3.1	Conventional LC VCO……..……..	8
3.2	Proposed quadrature voltage controlled oscillator……..……	9
3.3	Current recycling mechanism……..……	11
3.4	Comparison of amplitude between proposed and conventional QVCO……..……	13
3.5	Modeling of QVCO for mathematical analysis……...…	16
3.6	Quadrature catch up of proposed QVCO……..…..	18
3.7	Impedance plot of parallel RLC……..……	23
3.8	Quadrature phase error vs coupling factor for 0.1% tank mismatch……..	24
3.9	Quadrature phase error vs tank mismatch for coupling factor, m=0.148……...	24
3.10	Impact of coupling device mismatch on quadrature accuracy…	26
3.11	Impact of tank mismatch on quadrature accuracy……...	26

FIGURE Page

3.12	Impact of tank mismatch and coupling device mismatch on quadrature accuracy…….……....	27
3.13	Quadrature phase error vs coupling device mismatch (in %)…..	28
3.14	Waveforms at tail node……...…….	30
3.15	Phase noise comparison…….……..	32
4.1	Tank circuit…….…….....	33
4.2	Accumulation mode MOS varactor…….	34
4.3	Varactor Q vs V_{tune}……..……...	35
4.4	Symmetric center-tapped inductor……...……...….	36
4.5	Q and inductance vs frequency…….……..….	37
4.6	Modeling of tank losses……...	38
4.7	Tuning curve of the proposed QVCO……...……...	41
5.1	Layout of the proposed QVCO……..……..	43
5.2	Tuning characteristics of the proposed QVCO…….…..….	44
5.3	Phase noise of QVCO……..……	44
5.4	Monte Carlo simulation result for V_{tune} = 0.4 V…….….....	46
5.5	Monte Carlo simulation result for V_{tune} = 1.4 V……..…...	47
A.1	Modeling of LC oscillator under LC injection……...….	53

LIST OF TABLES

TABLE		Page
3.1	Sigma value for mismatch parameters……...	25
4.1	Device aspect ratio of Fig. 3.2…….……	40
5.1	Performance summary…….……..	45
5.2	Phase noise (at 1MHz offset) across corners…..……	45
5.3	Tuning range across corners……..	46
5.4	Performance comparison……...	48

CHAPTER I

INTRODUCTION

The rapid growth of modern wireless communication systems has generated increasing interest in high performance RF transceivers. Zero-IF and Low-IF architectures, which eliminate the need for external filtering, have turned out to be the most promising ones delivering high performance with high integration and low cost to meet the stringent requirements demanded by modern wireless standards.

To relax the noise requirement from baseband amplifiers and filters, RF front-end should be designed with as low noise as possible. This requires mixers with low noise figure and high linearity for RF demodulation. In addition, very low phase noise for the local oscillator is needed to prevent degradation of signal-to-noise ratio by the blocking signals.

Due to modern modulation schemes quadrature down-conversion is essential in Zero-IF and Low-IF receivers so that phase information is retained in the received signal. In Low-IF receivers, accuracy of quadrature signals and matching of components determine the amount of image rejection. Therefore, as one of the key components in high performance RF transceivers, fully integrated quadrature voltage controlled oscillator is critical to improve the overall performance of the system. Apart from RF transceivers, quadrature VCOs are also found to be useful in clock and data recovery systems where

---

This thesis follows the style of *IEEE Journal of Solid-State Circuits.*

low jitter performance can be obtained and twice the data rate clock can be locked using a quadrature VCO.

A. Goal of the research

Several techniques in coupled LC VCO architectures have been reported in literature for generating quadrature signals with better phase noise and quadrature accuracy, but less attention has been given to the power consumed by the coupling network. This research focuses on generation of quadrature signals at lower power consumption with similar or better phase noise compared to other quadrature VCO architectures. The proposed QVCO is designed in 0.18 μm CMOS technology with 6 metal layers. The QVCO is tunable from 2.61 GHz - 2.85 GHz with the worst case phase noise of -120 dBc/Hz at 1 MHz offset over the entire tuning range.

B. Thesis guide

A brief description of what is to follow in this thesis is given below. It is divided into five different chapters. Chapter II captures some background information on quadrature LC oscillator and existing techniques in literature. The core of the thesis is in Chapter III which gives a detailed description of the proposed QVCO, and some mathematical equations describing the QVCO are shown. Chapter IV deals with the design of the proposed QVCO and covers design insights of varactors, inductors and the VCO buffer. Post-layout simulation results are covered in Chapter V which is followed by conclusion.

CHAPTER II

BACKGROUND

Generating quadrature signals with low power and low area has always posed a great challenge for circuit designers over years. Some of the common techniques used to generate quadrature signals are as follows:

1. Polyphase filter or RC - CR network driven by voltage controlled oscillator (VCO),
2. Frequency division method,
3. Coupled LC oscillators.

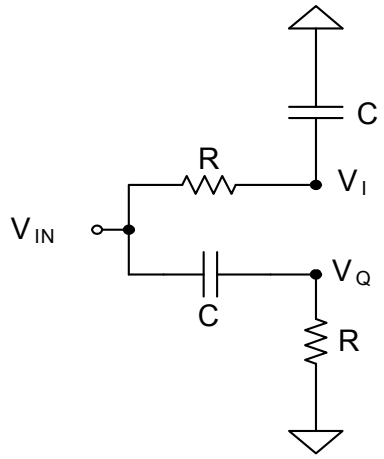

Fig. 2.1. RC-CR circuit for quadrature generation.

The first method (shown in Fig. 2.1) always maintains the phase difference between V_I and V_Q as 90°, but the amplitudes of the outputs differ significantly with frequency. The amplitudes of V_I and V_Q are equal only at their pole frequency of $\omega_p = 1/RC$. It requires

a buffer between VCO and filter to avoid loading effect, which increases power consumption heavily and degrades the phase noise of the quadrature signals. Variation in the absolute value of RC with temperature and process directly influences the value of the frequency at which there are quadrature signals with equal amplitude. To provide quadrature relationship over high bandwidth, two or more stages of RC-CR filter known as poly phase filter can be used. However, they suffer from significant attenuation and high (thermal) noise which cannot be ignored.

The frequency division method uses a master-slave flip-flop following a VCO running at twice the desired frequency. This method suffers from severe power consumption and the maximum achievable frequency is limited. Deviation in the input duty-cycle from 50% and mismatch in the signal paths would result in quadrature error. Two dividers can be employed to minimize the quadrature error but that would require input signal with four times the desired frequency. Both of the above discussed methods are open-loop architectures in which errors are directly propagated to the output.

As the focus of this research is on coupled LC VCOs, we look at them in more detail. In coupled LC oscillators, two symmetric LC VCOs are coupled to achieve quadrature outputs with good phase noise performance owing to LC oscillators. There are several ways to couple two LC VCOs which can be classified as direct injection and indirect injection.

In architectures like parallel coupled quadrature VCO (PQVCO) [1], coupling between two VCOs are done by direct injection method as shown in Fig. 2.2. The coupling

transistors $M_{2a} - M_{2b}$ are placed in parallel with the switching transistors $M_{1a} - M_{1b}$ and considerable amount of power is being used in coupling transistors which serve no purpose other than coupling signals from one LC core to the other. Moreover, there is a trade-off between quadrature accuracy and phase noise in such architectures.

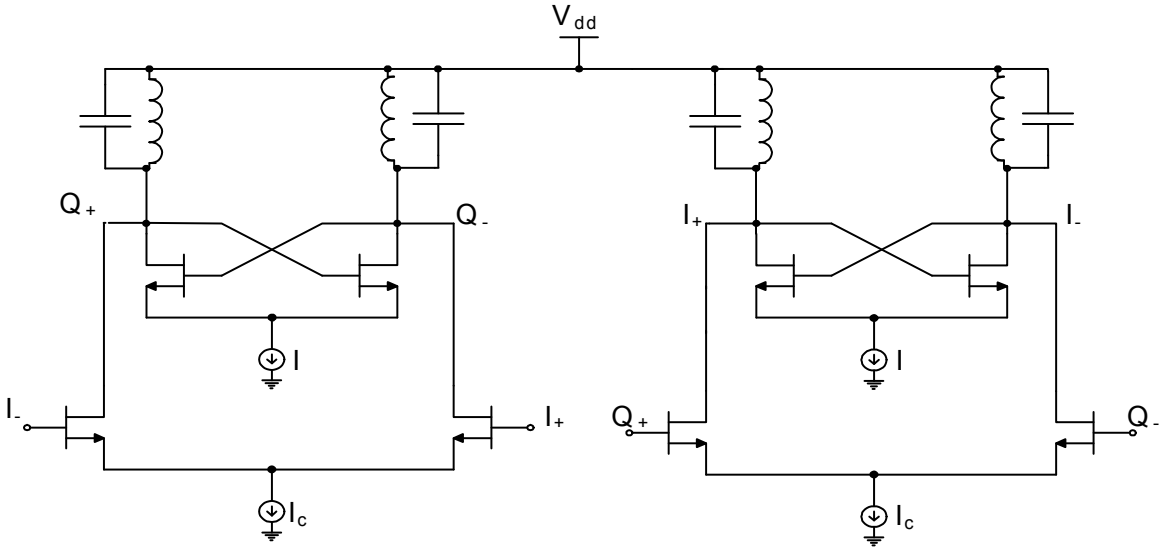

Fig. 2.2. Parallel coupled quadrature VCO (PQVCO).

Coupling the two LC VCOs by direct injection method pulls the two LC cores to oscillate a little away ($say\ \Delta\omega$) from their self resonant frequency (ω_0) such that the LC tank would contribute some phase shift to cancel the additional phase contributed by current injected from one LC core to the other through the coupling devices. As the frequency of oscillation is $\Delta\omega$ away from ω_0, there is some phase noise degradation in this architecture. Though this degradation can be eliminated by driving the coupling devices with additional 90° phase shifters [2], additional power consumption by the coupling devices is still a concern.

Its other variant, the series coupled quadrature VCO (SQVCO) [3] (shown in Fig. 2.3) uses the same bias current from the cross coupled pair and is reported to perform well in terms of phase noise. However, the coupling devices are five times larger than the switching devices, thus loading the oscillator with more parasitics and limiting the tuning range.

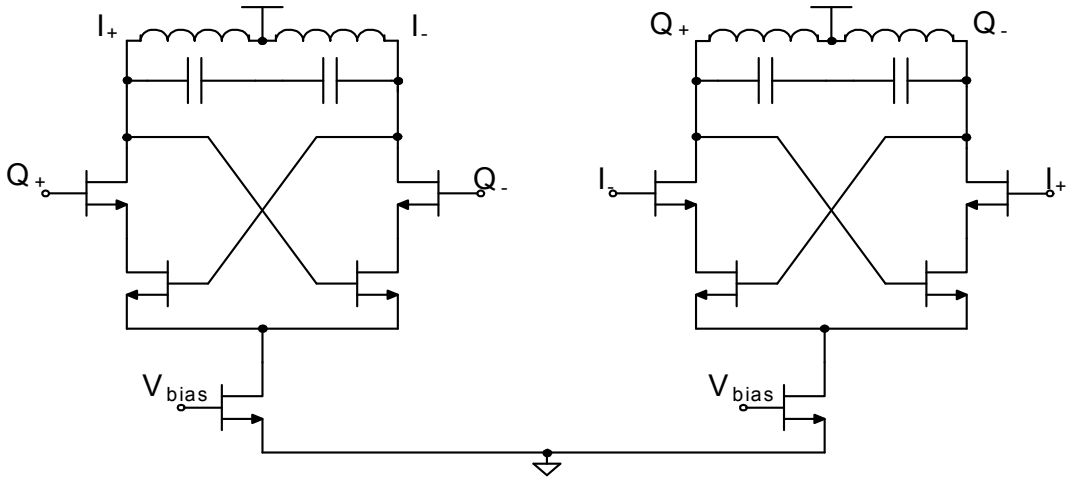

Fig. 2.3. Series coupled quadrature VCO (SQVCO).

Two LC VCO cores can also be coupled by indirect injection method (as shown in Fig. 2.4) in which super-harmonics of the fundamental oscillation frequency are used for coupling. This type of indirect injection enjoys several advantages (to be discussed later) over direction injection method. However, few of such oscillators reported in literature either use bulky components like inductors as shown in Fig. 2.4 or employ additional oscillator (running at $2\omega_0$) between the nodes v_{s1} and v_{s2}.

Though ring oscillators are capable of producing quadrature signals, they are not considered in RF transceivers because of their notorious phase noise performance.

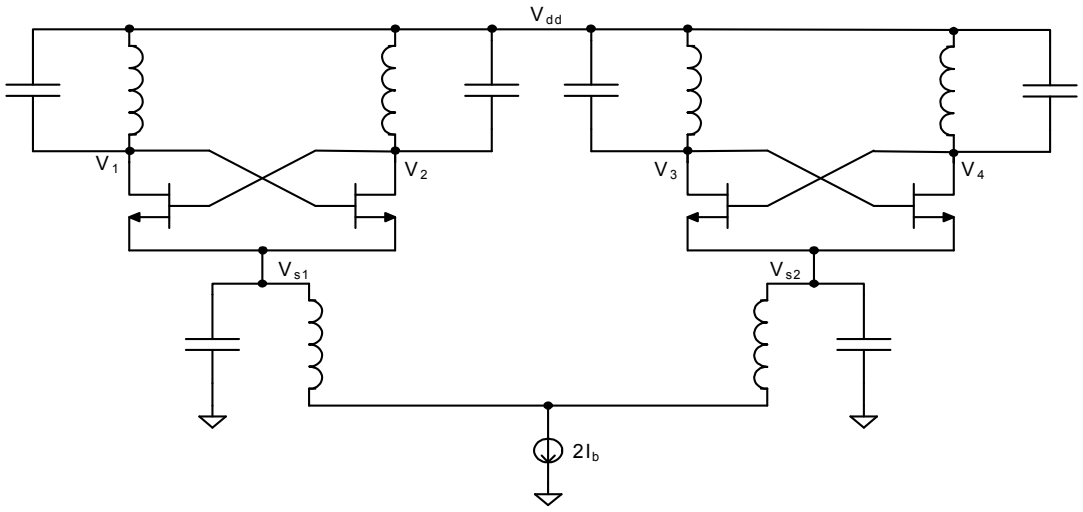

Fig. 2.4. Quadrature VCO using superharmonic coupling.

CHAPTER III

PROPOSED QUADRATURE VOLTAGE CONTROLLED OSCILLATOR

Differential coupling of second harmonic signal (say $2\omega_0$) between the common mode nodes of two differential oscillators running at their fundamental frequency ω_0 enables the two oscillators to run in quadrature [3].

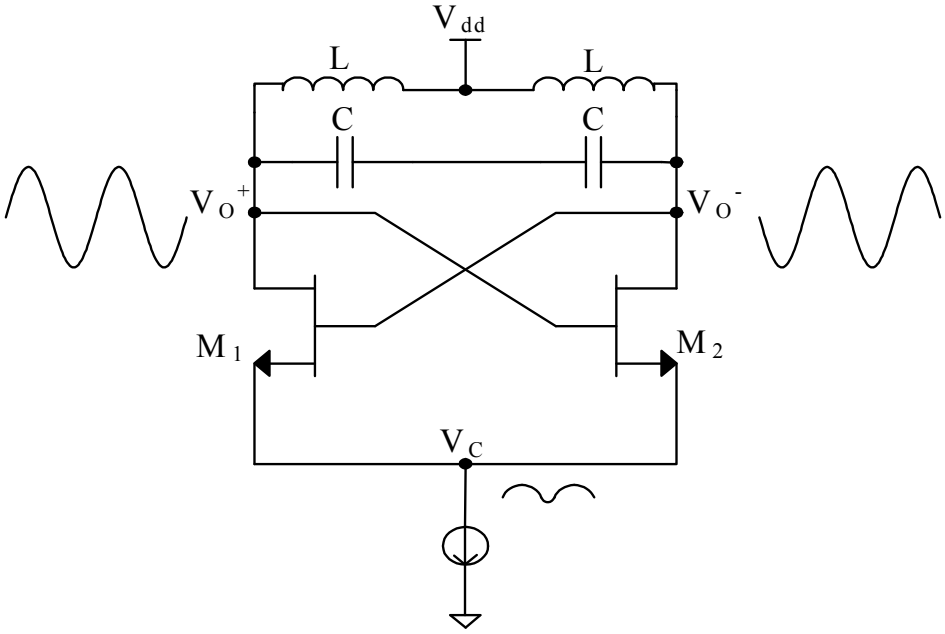

Fig. 3.1. Conventional LC VCO.

In a differential LC oscillator (as shown in Fig. 3.1), even harmonic signals (especially second harmonic) are predominantly found in the common mode node V_c. In a conventional single core LC VCO, it can be assumed that the large signal oscillating at the gates of the cross coupled differential pair switches them on and off at their zero crossings. Observation at the common source node (V_c) of this cross coupled differential

pair would reveal that the signal present at this node would be a full-wave rectified version of the large signal oscillating at their gates. The frequency relationship between the large oscillating signal and the full-wave rectified signal would be such that the latter would be at twice the frequency of the former.

This common source node (V_c) serves well for injecting signal at $2\omega_0$ from one LC core to the other in the case of coupled oscillators. Such indirect injection (at $2\omega_0$) between two LC cores is employed in the proposed architecture to achieve quadrature outputs.

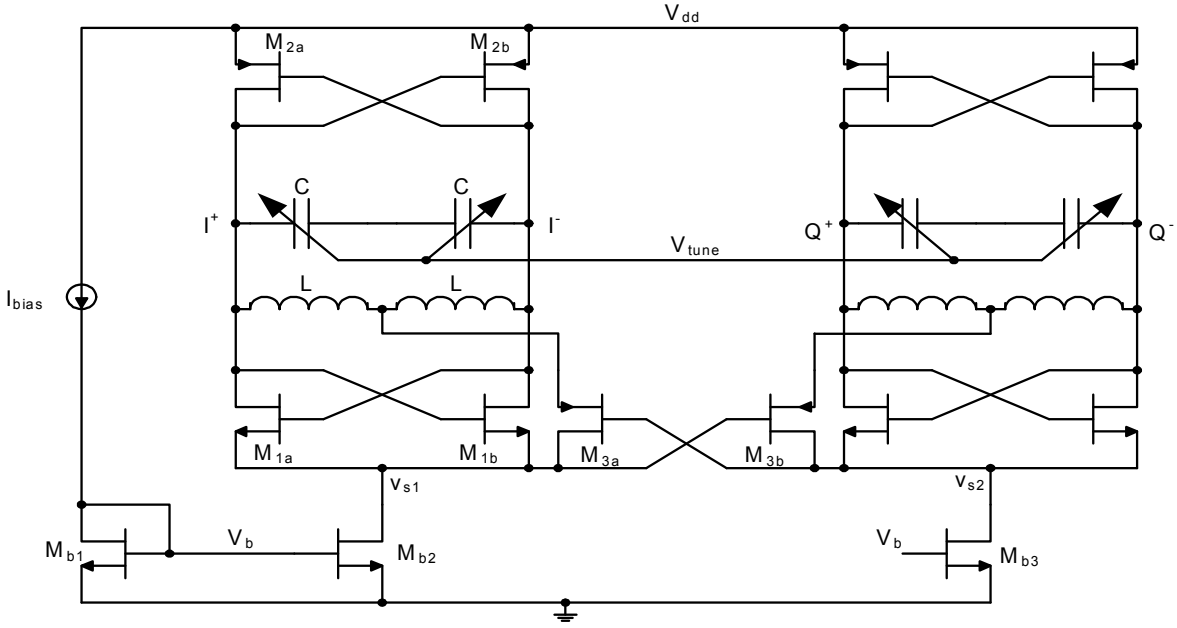

Fig. 3.2. Proposed quadrature voltage controlled oscillator.

The QVCO proposed in this work is shown in Fig. 3.2. Complementary cross coupled transistor pairs ($M_{1a} - M_{1b}\ and\ M_{2a} - M_{2b}$) in each LC core generate negative resistance to overcome the losses in the inductor L. Quadrature signals (I^+, I^-, Q^+, Q^-)

are generated to oscillate at $\omega_0\left(=1/\sqrt{LC}\right)$ by super harmonically (using second harmonic) coupling the two LC oscillators with their common mode nodes v_{s1} and v_{s2} as described above. This is achieved by another cross coupled transistor pair $M_{3a}-M_{3b}$ which pulls the $2\omega_0$ signals in v_{s1} and v_{s2} out of phase with each other to bring I^+, I^-, Q^+ and Q^- in quadrature.

The coupling devices $M_{3a}-M_{3b}$ has all its three terminals connected to the common mode nodes of the differential LC oscillator where even harmonic signals (predominantly second harmonic) are present with much smaller amplitude compared to the amplitude of the fundamental at I^+, I^-, Q^+, Q^- . Hence these coupling devices are expected to stay in saturation region throughout the signal swing.

The switching of the bias current by the cross-coupled devices $M_{1a}-M_{1b}$ and $M_{2a}-M_{2b}$ is shown pictorially in Fig. 3.3. It should be observed that the cross-coupled transistor pair $M_{3a}-M_{3b}$ recycles its bias current (I_b) back into the LC core through the center tap of the symmetrical inductor, which will be switched by the PMOS cross coupled transistor pair $M_{2a}-M_{2b}$ in both the cores. In addition to the tail current (I_a) being switched by the complementary cross coupled transistor pair which determines the amplitude of the oscillation at the fundamental frequency ω_0, additional switching of the coupling network's bias current (I_b) by the PMOS cross coupled transistor pair enhances the amplitude of oscillation across the LC tank. Hence the proposed coupling mechanism not only couples signals $(at\ 2\omega_0)$ from one LC core to the other to achieve quadrature

outputs, it also recycles its bias current back into the tank thereby saving power considerably.

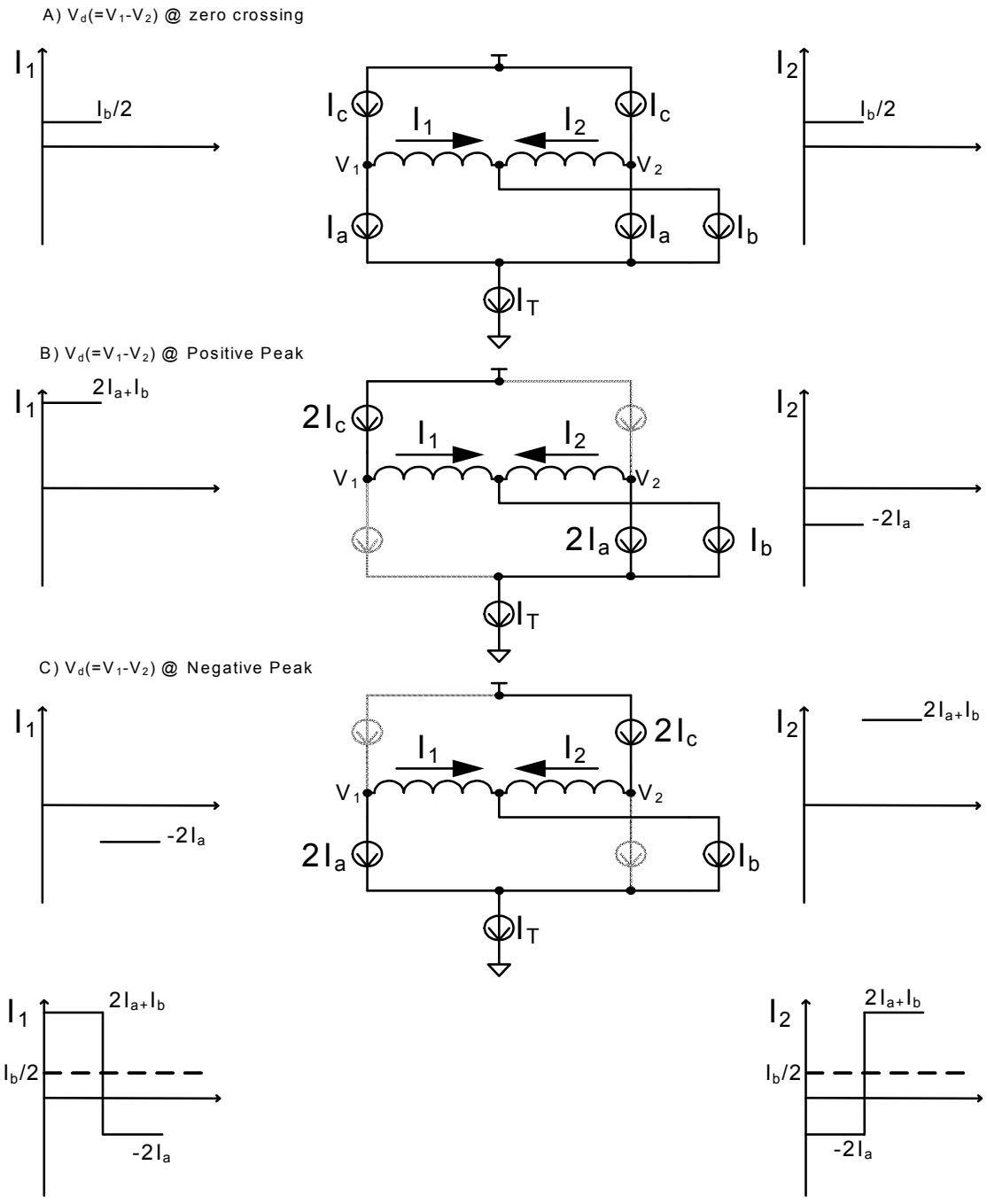

Fig. 3.3. Current recycling mechanism.

As shown in Fig. 3.3, I_a, I_b and I_c are the currents consumed by each of the transistor in the transistor pairs $M_{1a} - M_{1b}, M_{3a} - M_{3b}$ and $M_{2a} - M_{2b}$, respectively. Transistors in the circuit are replaced by the bias current consumed by them to have better insight for the current recycled by the coupling transistors. Let I_1 and I_2 be the current flowing through the inductors as shown in Fig. 3.3 which ultimately determine the amplitude of the oscillation. During the quiescent condition (when voltage swing V_d is at zero crossing),

$$I_1 = I_2 = I_b/2 \tag{3.1}$$

$$I_c = I_a + I_b/2 \tag{3.2}$$

To the first order, we can assume that the switching differential pairs $M_{1a} - M_{1b}$ and $M_{2a} - M_{2b}$ steer current from one arm to the other at zero crossing of V_d. When V_d is at positive peak (V_1 is high and V_2 is low), M_{1b} and M_{2a} are on and M_{1a} and M_{2b} are off. Since the coupling devices $(M_{3a} - M_{3b})$ are exposed to small swings $(@2\omega_0)$ it can be assumed that the current carried by them is relatively constant (I_b) compared to the current $I_{inj}(@2\omega_0)$. Since $I_T(= 2I_a + I_b)$ is fixed by the current mirror and M_{1a} is off, M_{1b} now carries the additional current I_a on top of I_a. Similarly, since M_{2b} is off, M_{2a} now carries $2I_c$. So the currents through the inductor are given by,

$$I_1 = 2I_a + I_b(= 2I_c) \tag{3.3}$$

$$I_2 = -2I_a \tag{3.4}$$

The same argument can be applied when V_d is at negative peak (V_1 is low and V_2 is high) which turns off M_{1b} and M_{2a} and turns on M_{1a} and M_{2b}. During this state the currents through the inductor are,

$$I_1 = -2I_a \tag{3.5}$$

$$I_2 = 2I_a + I_b \tag{3.6}$$

As shown in Fig. 3.3 the currents through the inductor switch from $2I_a + I_b$ to $-2I_a$ at the rate of ω_0, which determines the amplitude of oscillation. In the absence of coupling, as in the case of isolated conventional LC oscillator with complementary cross-coupled pairs [4], the current through the tank would have been switching from $2I_a$ to $-2I_a$. Hence the current consumed by the coupling network in the proposed QVCO contributes to the amplitude apart from coupling the two LC cores.

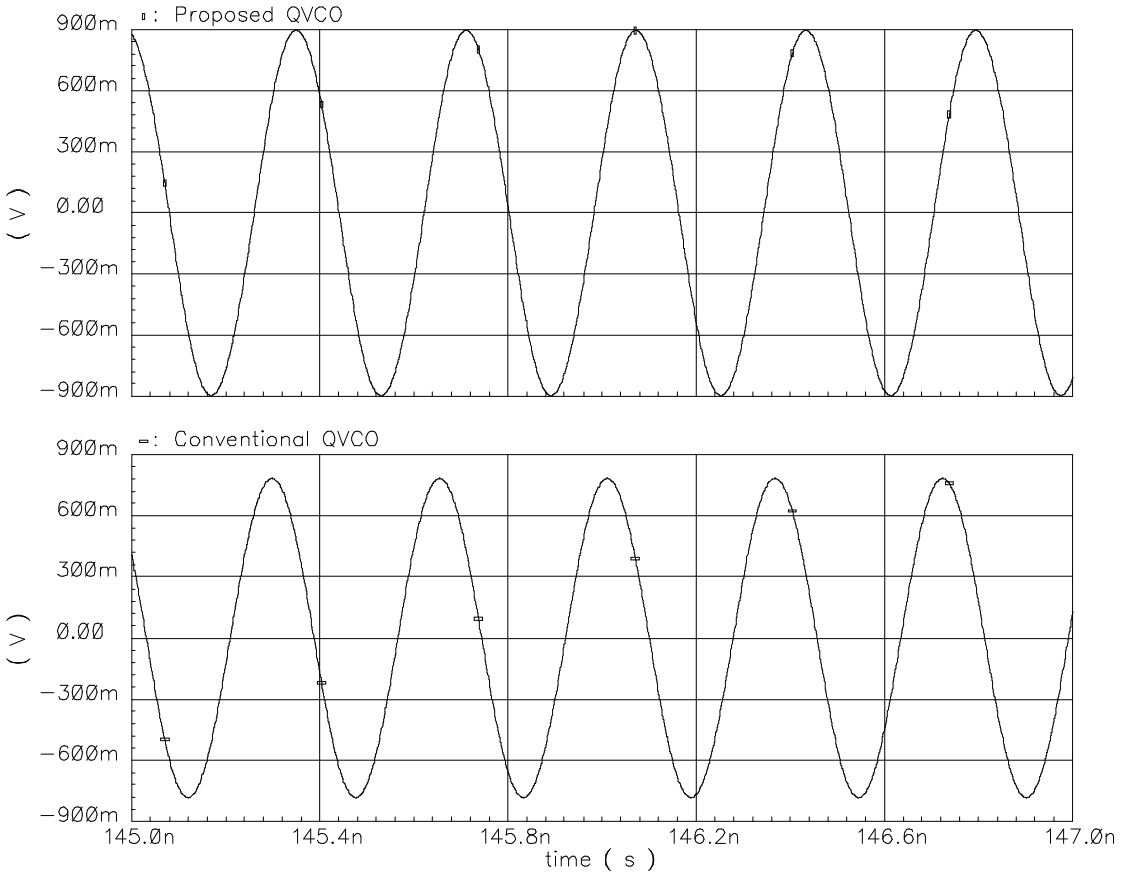

Fig. 3.4. Comparison of amplitude between proposed and conventional QVCO.

Though it is not exactly true that the switching pairs completely steer current from one arm to the other, similar analysis has been done on other conventional designs for comparison [5] and such an assumption gives acceptable results. The proposed QVCO has approximately 100 mV of higher amplitude compared to the conventional QVCO [1] for same power consumption as shown in Fig. 3.4.

In other conventional designs, the power consumed by the coupling network need not necessarily contribute to the amplitude of oscillation [1]. It is only the tail current of the primary LC core which predominantly determines their amplitude. In some designs, phase shifters were introduced between the two LC cores for better performance. However, these phase shifters complicate the design and increase the power consumption further. Apart from saving power, this additional bias current (from the coupling network) for the PMOS cross coupled transistor pair $M_{2a} - M_{2b}$ would help to keep the transistor (M_{2a-2b}) sizes low while designing for equal transconductance by NMOS and PMOS cross coupled pairs. Equal transconductance is desired to achieve symmetrical swing across the LC tank which would minimize the flicker noise upconversion, hence preventing close-in phase noise degradation [4]. By keeping the PMOS sizes low, its parasitics at the output nodes are reduced as well, enabling higher frequency of oscillation. Hence the proposed architecture ensures that the power consumed by the coupling network is negligible as it circulates the bias current back into the oscillator. The DC bias for the QVCO is provided by a simple current mirror M_{b1-b3} as shown in the Fig. 3.2. Since the oscillations at node v_{s1} and v_{s2} are at very higher frequency, it is possible that they get coupled to node X (or Y) due to the

parasitics between gate and source of M_{3a} (or M_{3b}). As X (or Y) is common mode node they do not disturb the differential output $I^+ - I^-$ (or $Q^+ - Q^-$) under the assumption that the inductors are perfectly matched.

The proposed quadrature oscillator is completely symmetric. So there is a possibility that one oscillator output leads or lags the other based on the initial conditions. Simple extra circuitry can be added to pre-determine the quadrature phase sequence.

A. Mechanism of quadrature operation

In this section, we mathematically analyze the operation of the quadrature LC VCO using differential equations. From the circuit shown in Fig. 3.2, it is clear that the PMOS cross coupled transistors are employed to switch the bias current I_{b0} to provide additional negative g_m for compensating the tank losses. This can be modeled as enhancement in Q of the tank and rest of the circuitry for single core is shown Fig. 3.5.

The tail current which is being switched by the NMOS cross-coupled differential pair is composed of the bias current I_{b0} and the injection current I_{inj} at 2ω from the other LC core.

$$I_t = I_{b0} + I_{inj}\cos(2\omega t + \theta_{inj}) \tag{3.7}$$

where $I_{inj} \ll I_{b0}$.

An assumption has been made on the operation of the differential pair that it completely steers the tail current from one arm to the other during the zero crossings of $V_{out}(t)$,

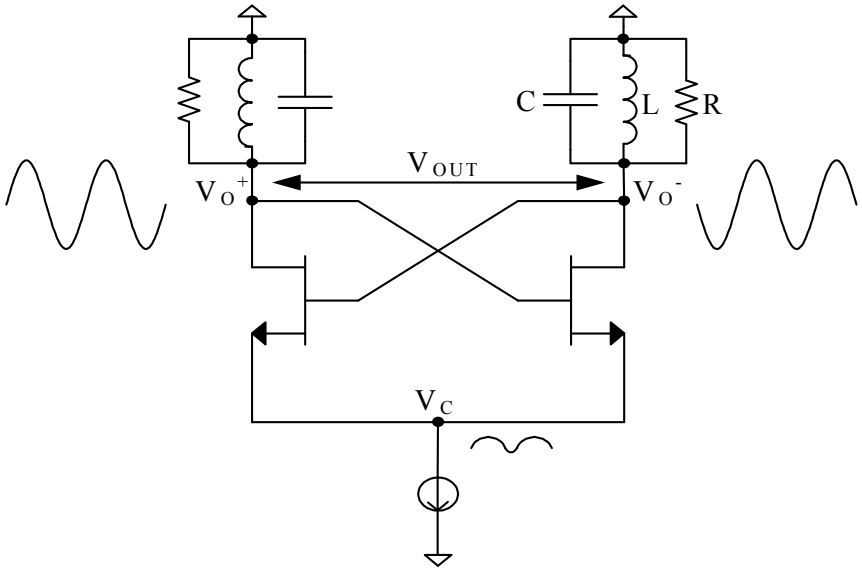

Fig. 3.5. Modeling of QVCO for mathematical analysis.

which is given by,

$$V_{out}(t) = V_I^+(t) - V_I^-(t) \tag{3.8}$$

Therefore, the differential current into the tank is represented as,

$$I_{out} = \text{sgn}(V_{out})I_t \tag{3.9}$$

Using Kirchhoff's current law at nodes I^+ and I^- and simplifying the equation yields the following result.

$$C\frac{d^2V_{out}}{dt^2} + \frac{1}{R}\frac{dV_{out}}{dt} + \frac{V_{out}}{L} = \frac{d}{dt}[\text{sgn}(V_{out})I_t] \tag{3.10}$$

In steady state, since the potential across the tank is of sinusoidal nature, we can assume the solution for the differential equation to be of the form,

$$V_{out} = V_a \cos(\omega t + \theta_{out}) \tag{3.11}$$

Expanding $\mathrm{sgn}(V_{out})$ in Fourier series, and considering the first two non-zero coefficients in the expansion (for simplification),

$$\mathrm{sgn}(V_{out}) = \frac{4}{\pi}\cos(\omega t + \theta_{out}) - \frac{4}{3\pi}\cos\big(3(\omega t + \theta_{out})\big) \tag{3.12}$$

Using (3.12) in (3.10), when $\omega = 1/\sqrt{\mathrm{LC}}$ we get two solutions (see Appendix I),

Case I: $\theta_{out} = \theta_{inj}/2$

$$V_a = \frac{4}{\pi} I_{b0} R \left[1 + \frac{m}{3}\right] \tag{3.13}$$

Case II: $\theta_{out} = \theta_{inj}/2 + \pi/2$

$$V_a = \frac{4}{\pi} I_{b0} R \left[1 - \frac{m}{3}\right] \tag{3.14}$$

where m is the coupling factor defined as I_{inj}/I_{b0}.

Intuitively, it can be concluded that among these two possible solutions the one with larger amplitude will exist [6]. When oscillations begin to grow up during initial cycles of oscillation, due to the non-linear amplitude control mechanism which is inherent LC oscillators with cross-coupled transistors, the mode with larger amplitude (3.13) will continue to grow while damping the mode with the smaller amplitude.

However, it must be observed that the oscillation frequency is $\omega = 1/\sqrt{LC}$ only when the electrostatic energy in the capacitor and the electromagnetic energy in the inductor are equal. In the presence of harmonics it is not true, as the current corresponding to these harmonics would flow chiefly into the capacitor increasing the electrostatic energy compared to that of the inductor. In order to the keep the energy in both arms equal, the

fundamental frequency must reduce itself with respect to $\omega = 1\sqrt{LC}$, so that the current through inductor increases in order to allow its electromagnetic energy to increase correspondingly [7].

The stable mode of operation bears the following phase relationship,

$$\theta_{out} = \theta_{inj}/2 \tag{3.15}$$

where θ_{inj} is the phase difference between the common mode signals at v_{s1} and v_{s2}. θ_{out} is the phase difference between the output waveforms V_I and V_Q.

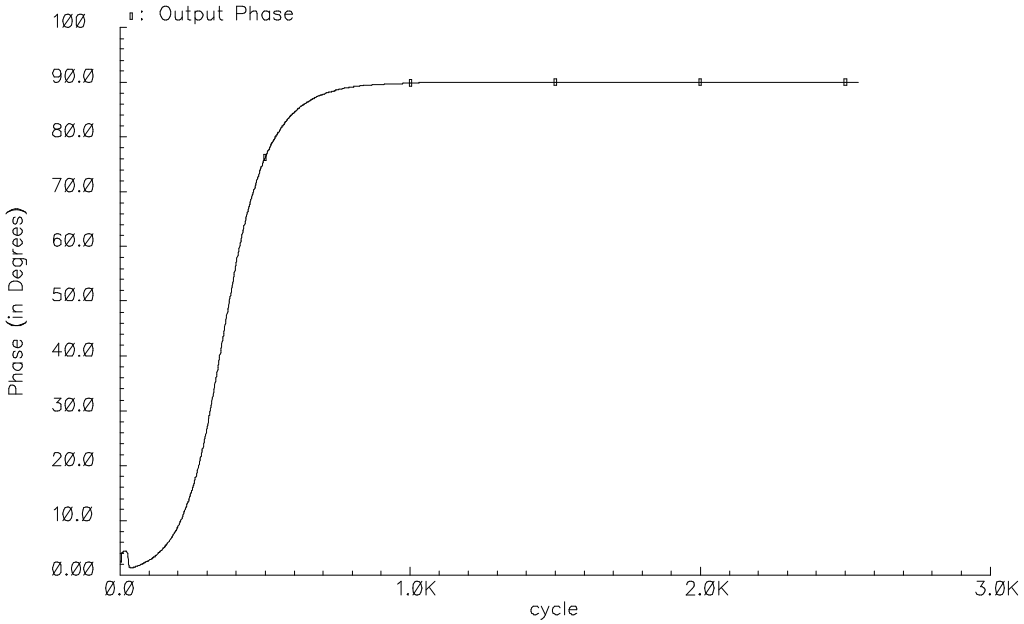

Fig. 3.6. Quadrature catch up of proposed QVCO.

Therefore, if θ_{inj} is forced to 180°, θ_{out} will be 90° hence V_I and V_Q will bear quadrature phase relationship. This is accomplished by the cross-coupled PMOS $M_{3a} - M_{3b}$ which pulls the $2\omega_0$ signals at v_{s1} and v_{s2} to be out of phase with each other

thereby achieving $\theta_{inj} = 180°$. The quadrature catch up during initial cycles of oscillation is shown in Fig. 3.6.

B. Quadrature inaccuracy due to mismatches

Mismatches between the two oscillator cores cause quadrature and amplitude error between the oscillator outputs. Amplitude mismatch is usually suppressed by the buffers following the oscillator cores, but the phase error propagates to the output completely thereby gathering more attention.

Mismatch between the oscillator cores is primarily because of the mismatch between the two LC tanks. This leads to different resonant frequencies in the LC tanks (say ω_{01} in oscillator I and ω_{02} in oscillator II). When oscillations start-up, the two tanks initially oscillate at their respective resonant frequencies and their common source nodes (v_{s1} and v_{s2}) oscillate at the second harmonic of their respective tank resonant frequencies. Due to the coupling between v_{s1} and v_{s2} by $M_{3a} - M_{3b}$, oscillator II oscillating at ω_{02} would inject current I_{inj} at $2\omega_{02}$ into the common source node of oscillator I. This would beat with ω_{01} and produce sinusoid at $(2\omega_{02} - \omega_{01})$ which is greater than ω_{01}. This would cause the oscillator I to increase its frequency of oscillation. Similar phenomenon occurs in oscillator II, where the signal injection from oscillator I into the tail node of oscillator II would cause it to decrease the frequency of oscillation. This beating takes place repeatedly until both the oscillators settle at a common oscillation frequency $\omega_{0c} \neq \omega_{01} \neq \omega_{02}$. Since this frequency of oscillation (at steady state) is away

from the natural frequency of the tank there will be some phase delay between the current injected into the tank and the corresponding voltage across the tank which would result in some quadrature inaccuracy between the outputs of the two oscillators. Apart from this, there will be slight degradation in phase noise as the oscillation frequency is not the natural frequency of the tanks.

Using Kirchhoff's current law at nodes I^+ and I^- and simplifying the equation yields the following result.

$$C\frac{dV_{out}}{dt} = \text{sgn}(V_{out})I_t + I_{Lout} - \frac{V_{out}}{R} \tag{3.16}$$

We know,

$$\theta_{out} = \frac{\theta_{inj}}{2} + \theta_e \tag{3.17}$$

$$V_{out} = V_a \cos(\omega t + \theta_{out}) \tag{3.18}$$

where θ_e is unknown phase error with respect to θ_{out} due to mismatches.

Using (3.17) and (3.18) in (3.16) and assuming $\theta_{inj} = 0$ (for simplicity),

$$-C\omega V_{out}\sin(\omega t + \theta_e) + \frac{1}{L\omega}V_{out}\sin(\omega t + \theta_e) = \text{sgn}(V_{out})I_t - \frac{V_{out}}{R} \tag{3.19}$$

Using (3.7) and (3.12) and neglecting the higher order harmonics,

$$\begin{aligned}\text{sgn}(V_{out})I_t = \frac{4}{\pi}I_{b0}\cos(\omega t + \theta_e) + \frac{2}{\pi}I_{inj}\cos(\omega t - \theta_e) \\ - \frac{2}{3\pi}I_{inj}\cos(\omega t + 3\theta_e)\end{aligned} \tag{3.20}$$

Due to the mismatches, the frequency error from ω_0 is defined as,

$$\Delta\omega = \omega - \omega_0 \tag{3.21}$$

Approximating the left side expression of (3.19),

$$\left(-c\omega V_{out} + \frac{1}{L\omega}V_{out}\right)\sin(\omega t + \theta_e) \cong (-2CV_{out}\Delta\omega)\sin(\omega t + \theta_e) \tag{3.22}$$

Assuming that the phase error θ_e is very small, we have $\sin(\theta_e) \cong \theta_e$ and $\cos(\theta_e) \cong 1$.

Balancing the harmonics in (3.19) leads to,

$$-2CV_{out}\Delta\omega + \left(\frac{4}{\pi}I_{b0} - \frac{V_a}{R} - \frac{4}{\pi}I_{inj}\right)\theta_e = 0 \tag{3.23}$$

$$\frac{4}{\pi}I_{b0} - \frac{V_a}{R} + \frac{4}{3\pi}I_{inj} = 0 \tag{3.24}$$

Solving for V_a from (3.24),

$$V_a = \frac{4}{\pi}I_{b0}R\left[1 + \frac{m}{3}\right] \tag{3.25}$$

which is same as (3.13), hence V_a remains constant even if the tank are mismatched.

Solving for θ_e from (3.23) reveals that,

$$\theta_e = \left(\frac{-2CV_a}{I_{inj}\frac{16}{3\pi}}\right)\Delta\omega \tag{3.26}$$

Assuming the tank mismatches have affected the output phase of both the oscillator cores, the voltages across the tanks can be represented as,

$$V_I = V_a\cos(\omega t + \theta_{out1}) \tag{3.27}$$

$$V_Q = V_a\cos(\omega t + \theta_{out2}) \tag{3.28}$$

From (3.17),

$$\theta_{out1} = \frac{\theta_{inj1}}{2} + \theta_{e1} \tag{3.29}$$

$$\theta_{out2} = \frac{\theta_{inj2}}{2} + \theta_{e2} \tag{3.30}$$

Assuming $\theta_{inj1} = 0°$ and $\theta_{inj2} = 180°$, the quadrature error is obtained as,

$$\theta_e = 90° - (\theta_{out2} - \theta_{out1}) \tag{3.31}$$

$$\theta_e = \theta_{e1} - \theta_{e2} \tag{3.32}$$

where $\theta_{e1} = \left(-2CV_a/I_{inj}\frac{16}{3\pi}\right)(\omega - \omega_{01})$ and $\theta_{e2} = \left(-2CV_a/I_{inj}\frac{16}{3\pi}\right)(\omega - \omega_{02})$.

Substituting for θ_{e1} and θ_{e2} in (3.32) we have,

$$\theta_e = \left(\frac{2CV_a}{I_{inj}\frac{16}{3\pi}}\right)(\omega_{01} - \omega_{02}) \tag{3.33}$$

Substituting for V_a from (3.26), we get the quadrature inaccuracy to be,

$$\theta_e = \frac{\frac{3}{2}Q\left(\frac{1}{m} + \frac{1}{3}\right)(\omega_{01} - \omega_{02})}{\omega_0} \tag{3.34}$$

Though high Q resonant circuits result in good phase noise performance, such high Q's will result in more phase variation versus frequency (shown in Fig. 3.7), which contributes heavily to quadrature inaccuracy in the case of mismatches as seen in (3.34). From (3.34), it can also be observed that having higher coupling factor ($m = I_{inj}/I_{b0}$), minimizes quadrature error to some extent. The amount of mismatch between the two

oscillator cores is captured in $(\omega_{01} - \omega_{o2})$ term. Similar mismatch analysis has been done in [8] for quadrature VCOs.

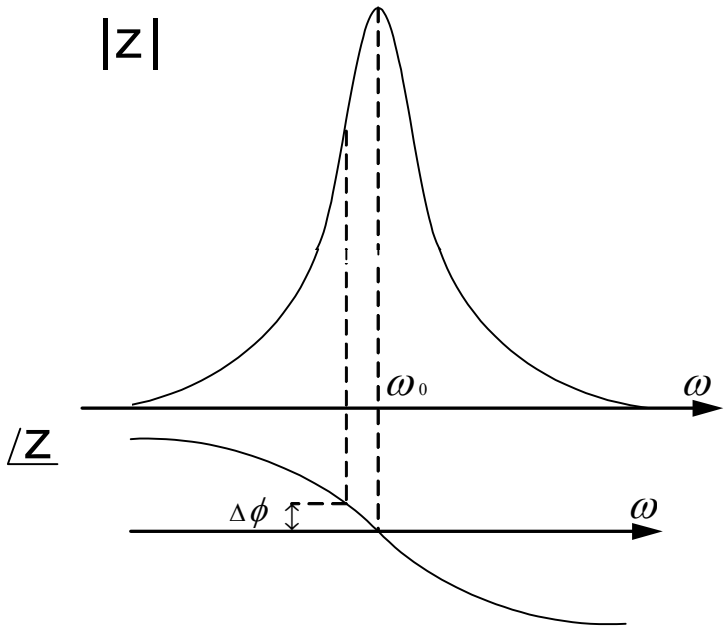

Fig. 3.7. Impedance plot of parallel RLC.

The empirical formulae for the design of integrated spiral inductors [9] suggest that the overall inductance is generally insensitive to the width and thickness of the metal stripes to such an extent that the total size of the inductor remains the same. To model the tank mismatch, 0.1% mismatch has been introduced between the MIMCAP (Metal-Insulator-Metal Capacitor) structures in the proposed QVCO and the quadrature phase error has been obtained by simulation. Fig. 3.8 shows the simulated and theoretical quadrature phase error due to mismatch between the two LC tanks.

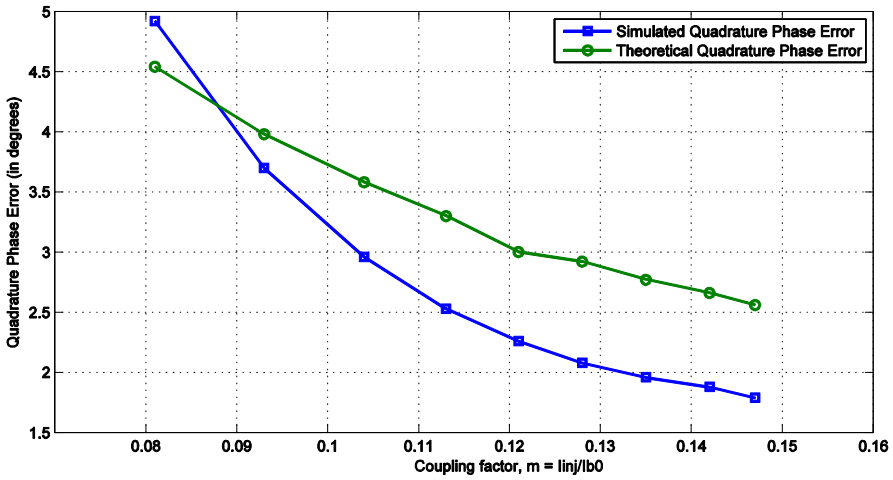

Fig. 3.8. Quadrature phase error vs coupling factor for 0.1% tank mismatch.

Similarly, the quadrature phase error was observed across varying levels of tank mismatches for a given coupling factor m. For $m = 0.148$, tank mismatch was varied from 0.1% to 0.5% and the simulated quadrature phase error was compared against the theoretical quadrature phase error as shown in Fig. 3.9.

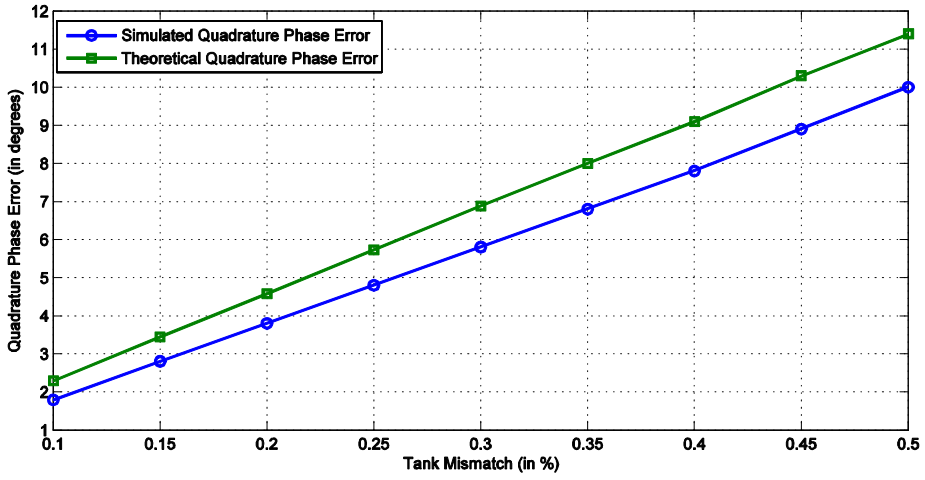

Fig. 3.9. Quadrature phase error vs tank mismatch for coupling factor, $m = 0.148$.

To analyze phase error contribution from the coupling devices $M_{3a} - M_{3b}$, Monte Carlo simulation was ran to study mismatch effects of coupling devices on the quadrature phase. Random variations in Gaussian distribution of the process parameters including threshold voltage (V_{TH0}), device sizes (L and W) and oxide thickness (T_{OX}) are included in the model to account for mismatch performance.

Based on the size of the coupling devices the standard deviation of the process parameters are shown in Table 3.1.

Table 3.1. Sigma value for mismatch parameters.

Mismatch Parameter	**Standard Deviation**
σ_{VTH0} (mV)	1.274
$\sigma_{XL/L}$ (%)	0.118
$\sigma_{XW/W}$ (%)	0.100
σ_{TOX} (%)	0.025

Fig 3.10 shows the output phase relationship of the proposed QVCO in the presence of coupling device mismatch alone, while other components are perfectly matched. Since the tanks are perfectly matched, $\omega_{01} = \omega_{02}$ in (3.34), which would theoretically result in zero quadrature phase error. However, the mismatch between the coupling devices would add different parasitics to the two LC cores and would inject different super-harmonic current into each core which would cause non-zero quadrature phase error. From Fig 3.10, it can be observed that the standard deviation from the mean value of the

output phase is very low and the mismatch between the coupling devices does not cause any severe degradation in the performance.

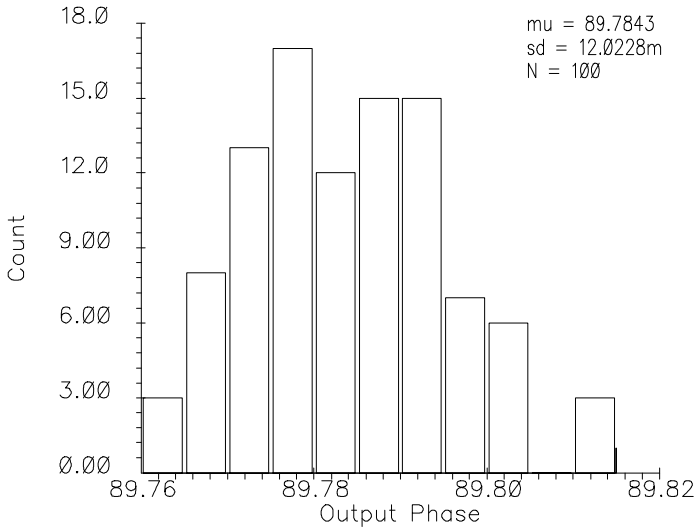

Fig 3.10. Impact of coupling device mismatch on quadrature accuracy.

Similar Monte Carlo simulation was performed to observe the effect of MIMCAP mismatch on the quadrature phase error. Mismatch model for MIMCAP alone was inclu-

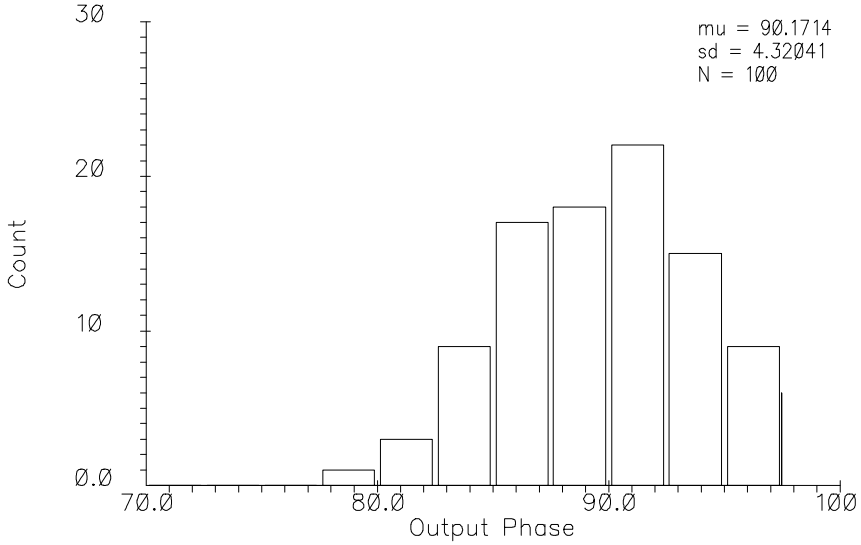

Fig 3.11. Impact of tank mismatch on quadrature accuracy.

ded in the simulation, while other components were kept matched. For mean value of 1.02 pF, the standard deviation of the MIMCAP was observed to be 51.8 fF and this had adverse effect on the quadrature output phase as shown in Fig. 3.11. The standard deviation of the quadrature phase error caused by MIMCAP mismatch alone is 4.32° and that due to coupling device mismatch alone is 0.012°, from which it is clear that mismatch between the MIMCAPs have detrimental effect on the performance of the QVCO and the mismatch effect of the coupling devices is negligible. To validate this further, Monte Carlo simulation was performed with mismatch models for both the MIMCAPs and the coupling devices included in the simulation. The resulting quadrature phase error has been captured in Fig. 3.12 which shows the standard deviation of the output phase error to be 4.33°, almost same as the one due to MIMCAP mismatch alone.

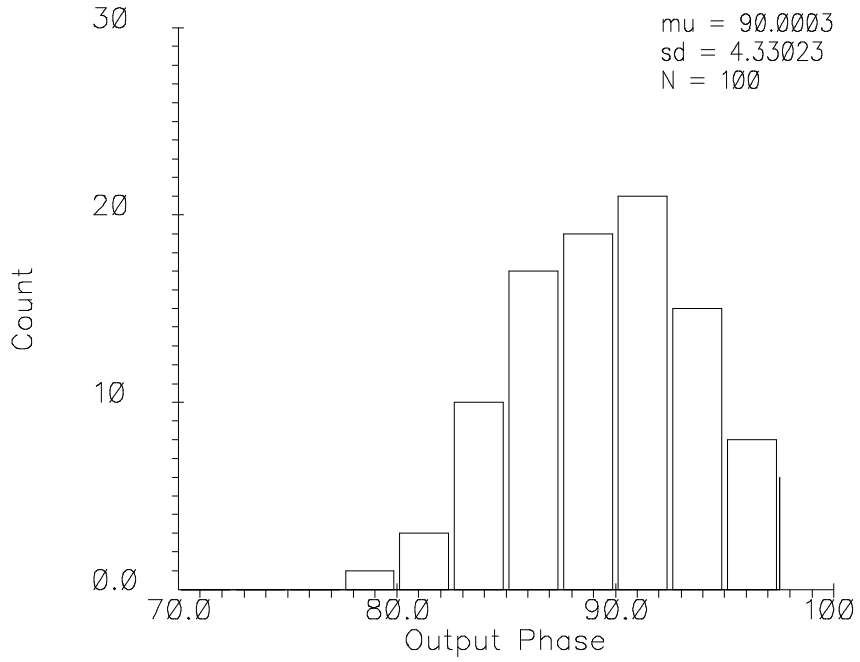

Fig 3.12. Impact of tank mismatch and coupling device mismatch on quadrature accuracy.

Hence, the mathematical analysis which assumes the mismatch between coupling transistors to be negligible and takes into account only the mismatch between the LC tanks in the two cores seems to be more valid assumption.

Apart from random mismatch analysis, deterministic mismatches were added to the coupling devices ($M_{3a} - M_{3b}$) to analyze their phase error contribution. As shown in Fig. 3.13, we see that, their contribution to the quadrature phase error is very less even for large amount of mismatch whereas the quadrature phase error is highly sensitive to mismatch between tanks, even if the mismatch is as low as 0.1% (see Fig. 3.8).

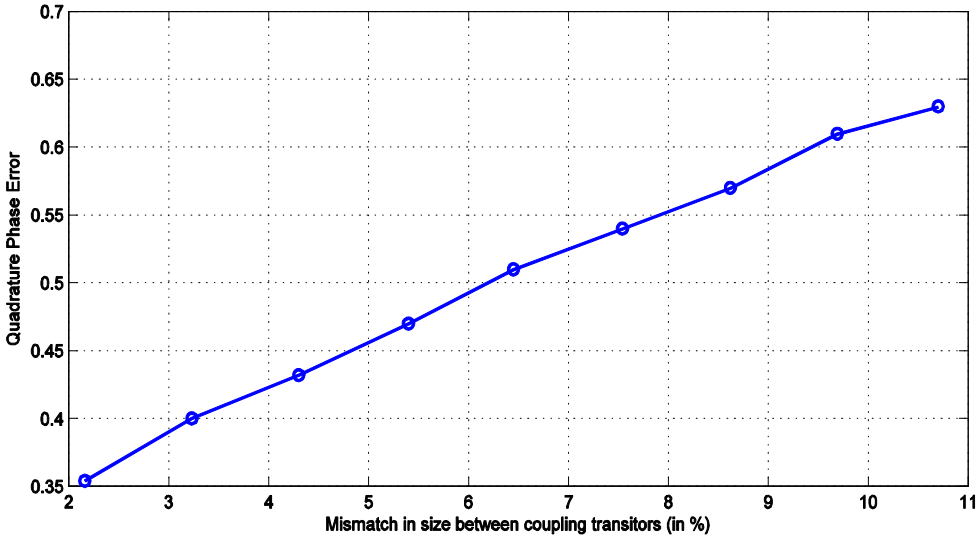

Fig. 3.13. Quadrature phase error vs coupling device mismatch (in %).

C. Phase noise analysis

During steady state operation the cross-coupled transistors $M_{1a} - M_{1b}$ and $M_{2a} - M_{2b}$ are exposed to large signal swings at the nodes I^+ and I^- (see Fig. 3.2) which switch

them on and off periodically at the rate of ω_0. When the node I^+ is high (and I^- is low) M_{1a} will be switched off, M_{1b} will be switched on in the triode region and vice versa when I^+ is low (and I^- is high). The cross-coupled pair $M_{1a} - M_{1b}$ can be sized to keep their r_{ds} small enough to consider the nodes I^+ and I^- shorted to v_{s1} through M_{1a} and M_{1b}, respectively, when they operate in deep triode region. This makes the frequency of oscillation at the tail node v_{s1} to be $2\omega_0$ as shown in Fig. 3.14.

When one of the transistors in the cross-coupled pair $M_{1a} - M_{1b}$ is switched off while the other is operating in triode region, noise cannot flow into the tank as the transistor which is on is assumed to be cascoded by the current source M_{b2} (assuming the parasitics at the tail node to be small). So, when the transistor is in deep triode region most of the noise current circulates within the transistor [10].

When I^+ and I^- are equal (or during zero crossings of V_{out}), all the transistors are assumed to be operating in saturation region. This is when all the switching transistors inject noise into the tank, contributing heavily to the phase noise. As explained in [11], the LC oscillator is highly sensitive to the noise fluctuation at this instant of oscillation which results in permanent phase shift of the output signal.

Around the zero crossing point, the tail node v_{s1} (see Fig. 3.2) moves closer to the zero crossing voltage and this results in reduction of v_{gs} of the cross coupled pair $M_{1a} - M_{1b}$ and their g_{ds}. As a consequence of this, thermal noise generated by the transistors are reduced.

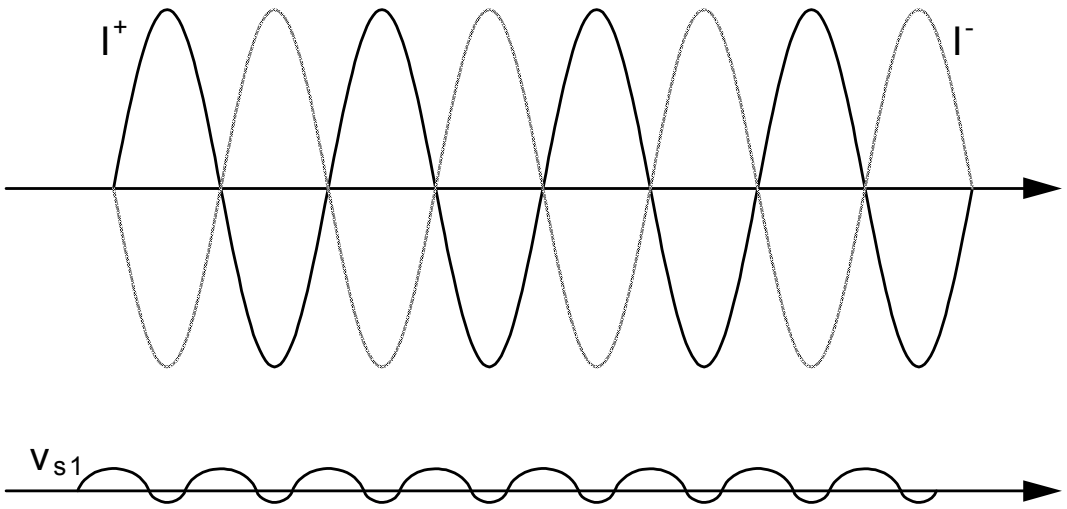

Fig. 3.14. Waveforms at tail node.

Compared to other conventional quadrature VCOs, the proposed QVCO is expected to achieve higher amplitude of oscillation for the same power consumption. The amplitude of oscillation for the conventional QVCO [1] and the proposed QVCO for the same power consumption is shown in Fig 3.4. This would result in better phase noise as it is referred to the power of the fundamental. According to the impulse sensitivity function (ISF) theory developed by Lee and Hajimiri [12], the phase noise $\left(\mathcal{L}(\Delta\omega)\right)$ of LC oscillator due to white noise sources is given by,

$$\mathcal{L}(\Delta\omega) = 10\log\left(\frac{\overline{i_n^2}}{\Delta f}\frac{\Gamma_{rms,n}^2}{2q_{max}^2\Delta\omega^2}\right) \tag{3.35}$$

where $i_n^2/\Delta f$ is the power spectral density (PSD) of the white noise current i_n, $\Gamma_{rms,n}^2$ is the root mean square value of the effective ISF associated to i_n, q_{max} is the maximum charge swing across the tank capacitance which depends on the amplitude of the oscillation and $\Delta\omega$ is the offset angular frequency from the ω_o.

From the phase noise expression in (3.35), it is clear that higher the amplitude of oscillation, better will be the phase noise at the same offset frequency. Hence the proposed architecture ensures better phase noise for the same power consumption compared to the conventional QVCO [1] as shown in Fig 3.15. When the amplitude of oscillation is more, the slope with which the waveform crosses the zero-crossing point will be high. As the slope is higher, the duration for which all the transistors remain in saturation around the zero-crossing point is shorter. This reduces the total noise energy being injected into the tank thereby reducing the phase noise of the QVCO.

The proposed QVCO enjoys similar advantage as other Superharmonic QVCOs. Indirect coupling of super harmonic signals in the common mode v_{s1} and v_{s2} ensures that the phase noise is not degraded, as tank circuit is not affected directly and it enables the circuit to oscillate at ω_0 as against direct coupling QVCOs which pulls the LC core to oscillate a little away from ω_0 to achieve quadrature outputs. The noise contribution by the coupling device is similar to the behavior of the tail current noise. However, the coupling device being PMOS has lesser flicker noise for up-conversion by the cross-coupled pair $M_{1a} - M_{1b}$, preventing phase noise degradation to some extent. This up-converted flicker noise enters the tank as AM noise and will not appear as phase noise unless the varactor has high gain to convert this AM to FM. At lower offset frequency, the flicker noise of the active devices contributes heavily to the phase noise of QVCO. The conventional QVCO [1] employs two pairs of NMOS coupling devices which

degrade the close-in phase as shown in Fig. 3.15. At higher offset frequency, the dominance of flicker noise disappears gradually and thermal noise begins to dominate.

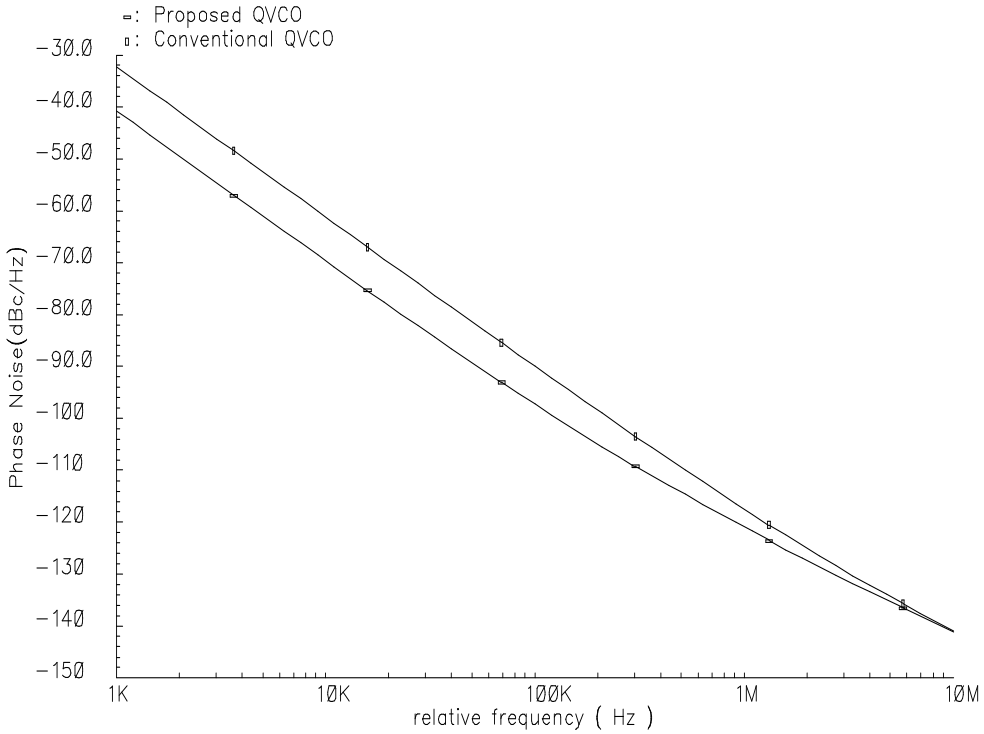

Fig. 3.15. Phase noise comparison.

CHAPTER IV

DESIGN OF QUADRATURE VOLTAGE CONTROLLED OSCILLATOR

The tank circuit shown in Fig. 4.1 is used in each of the oscillator cores to generate quadrature signals. It employs differentially driven symmetric center-tapped (CT) inductor L and fixed capacitor C_{fixed} which determines the center frequency of the osci-

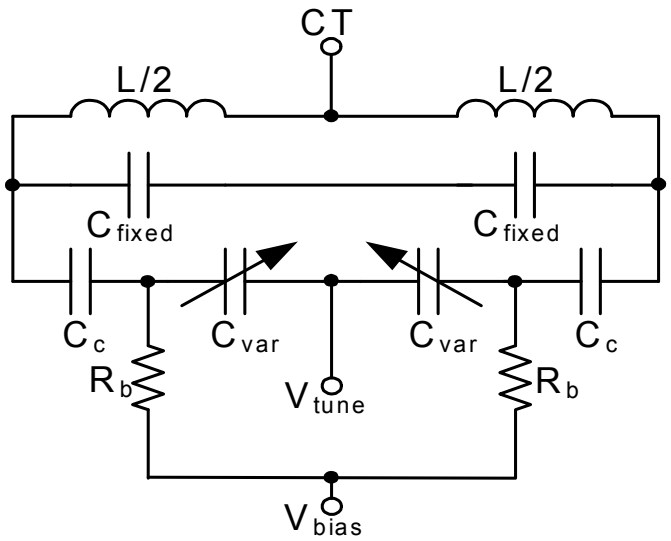

Fig. 4.1. Tank circuit.

-llator. C_{var} is the capacitance of the varactor which is tuned by the tuning voltage V_{tune} and C_c is the coupling capacitance. The fixed capacitor C_{fixed} is made of metal-insulator-metal (MIM) capacitors to preserve linearity in the output waveform.

A. MOS varactor

Accumulation mode MOS varactors [13] are used for C_{var}. MOS varactor is realized in n-well, with n^+ source and drain regions as shown in Fig. 4.2. This is done to prevent the injection of holes to inhibit the formation of inversion regions. Placing n^+ contacts in the place of source and drain regions minimize the parasitic n-well resistance.

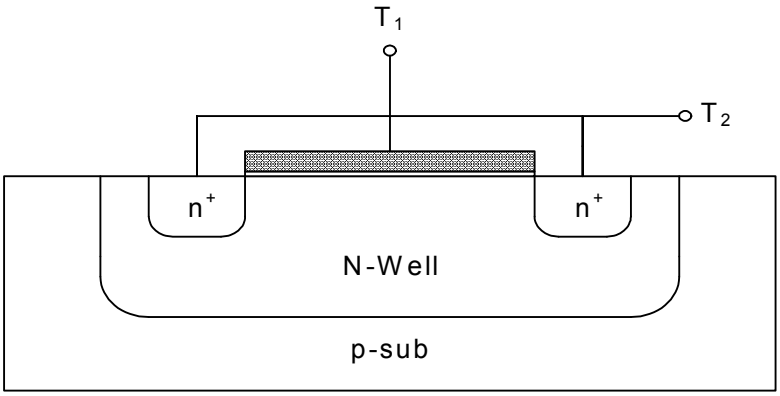

Fig. 4.2. Accumulation-mode MOS varactor.

Since MOS varactors possess high C_{max}/C_{min} ratio, they are used to tune the frequency of the QVCO. Multi-fingered and folded layout is used to minimize the gate resistance to obtain high quality factor (Q) so that the overall Q of the tank is dominated by the inductor whose quality factor is lesser than the MOS varactors. Simulation of varactor Q vs V_{tune} (see Fig. 4.3) shows high quality factor for the MOS varactor. Overall Q of the tank is given by,

$$\frac{1}{Q} = \frac{1}{Q_L} + \frac{1}{Q_C} \tag{4.1}$$

where Q_L is quality factor of the inductor and Q_C is the quality factor of the capacitor.

The oscillator has a very large swing across the inductor and connecting the varactor directly to the inductor terminals would cause the effective tuning voltage to vary periodically at the oscillation frequency. To the first order, it can be approximated that the effective capacitance of the varactor is the time-average capacitance over each oscillation period.

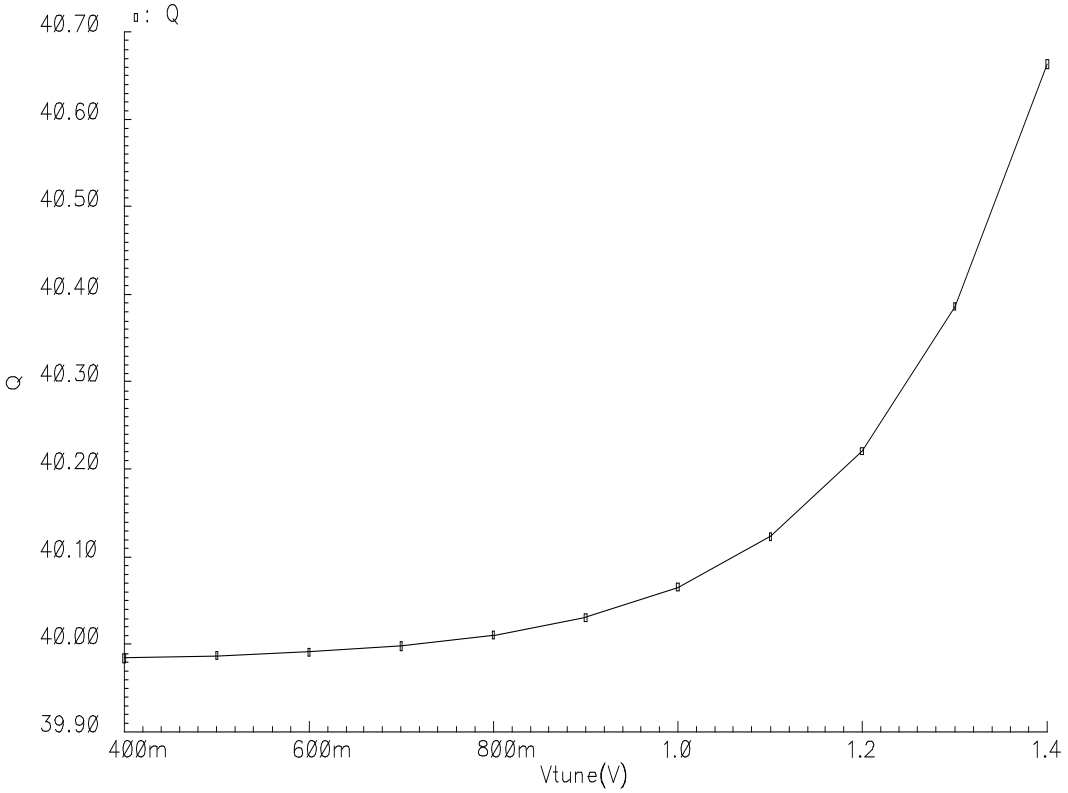

Fig. 4.3. Varactor Q vs V_{tune}.

Detailed analysis in [14] reveals that the effective capacitance not only depends on the average capacitance but also on the second-order Fourier coefficient of the non-linear varactor exposed to the oscillation. In addition to this, the effective capacitance of the varactor not only depends on the tuning voltage, but also on the amplitude of the

oscillation. To minimize the sensitivity of the varactor to the oscillation amplitude and to linearize the $C - V$ curve of the varactor, a fixed capacitor can be connected in series with the varactor (as shown in Fig. 4.1) at the expense of tuning range. External bias V_{bias} is given to the varactor through R_b.

B. Center-tapped inductor

Fully symmetric differentially driven center-tapped spiral inductors (as shown in Fig. 4.4) are used in the design of QVCO. Due to differential excitation, voltages on adjacent strips are out of phase, but current flow is in same phase which enhances the mutual coupling and provides more inductance per unit area [11].

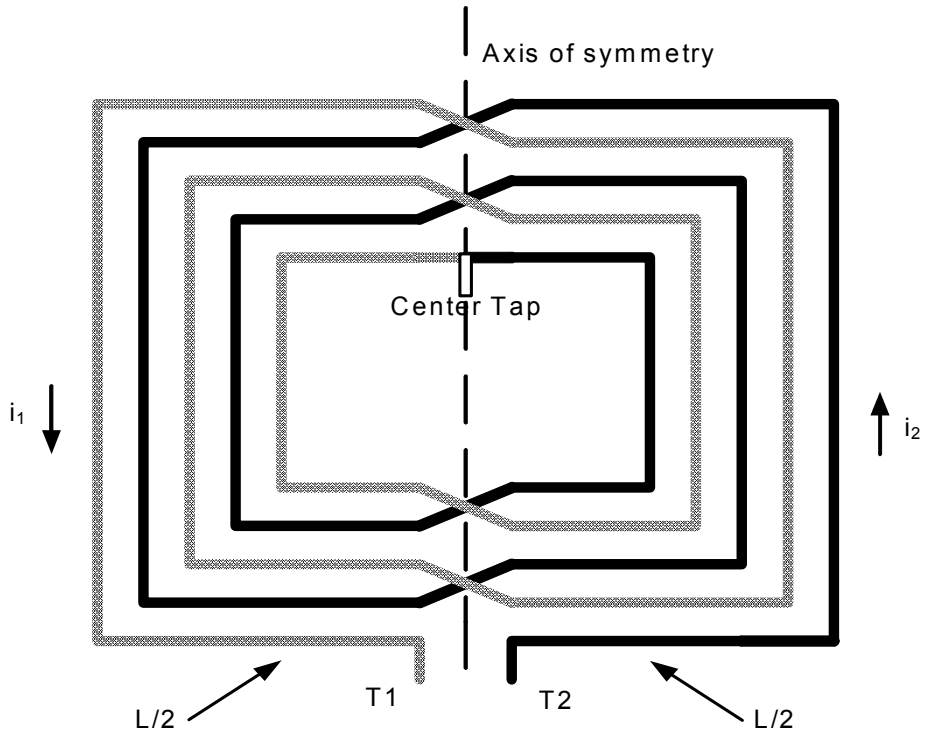

Fig. 4.4. Symmetric center-tapped inductor.

In differential excitation, the substrate parasitics present a higher equivalent shunt impedance compared to single-ended excitation as the substrate parasitics at both the nodes T_1 and T_2 are taken into account. This enhances Q of the inductor (when driven differentially) and the self-resonant frequency as the effective parasitic capacitance across the inductor is now reduced.

A three turn octagon shaped center-tapped inductor measuring 3.59 nH made using metal 6 (for minimum resistive loss), which is 300 μm wide, is used in each of the LC core. The simulated inductance and quality factor of the inductor is shown in Fig. 4.5.

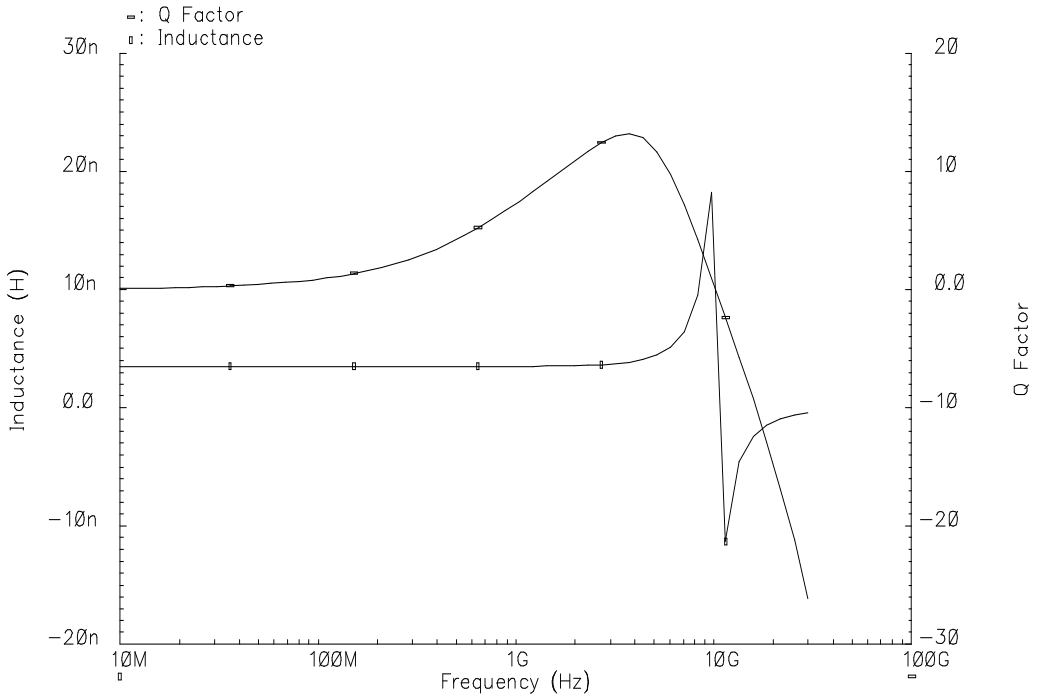

Fig. 4.5. Q and inductance vs frequency.

C. Cross-coupled transistors

As shown in Fig. 3.2, PMOS and NMOS cross-coupled differential pairs are used to compensate for the losses from the inductor. Usage of both PMOS and NMOS provides more negative g_m for a given current, though there will be limitation on the maximum amplitude of oscillation compared to the NMOS-only or PMOS-only LC VCO architectures. As the complementary architecture enables us to achieve symmetrical rise time and fall time for the generated signal, the ISF for such oscillators can be more symmetrical which keeps their DC component (DC coefficient in Fourier series expansion) to near zero. Designing oscillator with such symmetry (for ISF) minimizes the flicker noise upconversion from the tail node to around the carrier frequency.

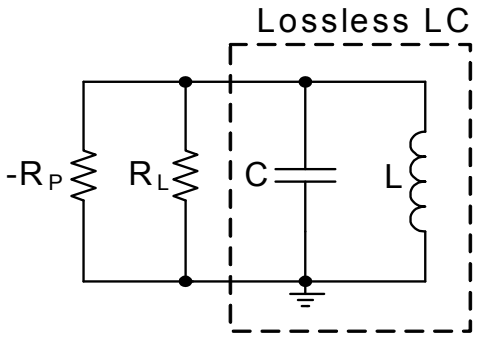

Fig. 4.6. Modeling of tank losses.

The tank losses which are predominantly due to series resistance R_s of inductor have been represented as a resistance R_L in parallel with the lossless tank LC in Fig. 4.6. Generally quality factor of the varactor (Q_c) is higher than that of the inductor (Q_L).

From (4.1),

$$Q \approx Q_L \tag{4.2}$$

and we have,

$$R_L = (1 + Q^2)R_S \approx Q^2 R_s. \tag{4.3}$$

In this design, we have $L = 3.59$ nH and $Q = 11.8$ which translates to $R_L = 638.48\ \Omega$.

As a rule of thumb, to overcome the loss due to R_L we need,

$$\frac{1}{R_P} > 2\frac{1}{R_L} \tag{4.4}$$

The inductance value was chosen based on the design strategy given in [15]. Smaller inductance results in better phase noise, but it cannot be indefinitely small as it will violate the minimum required oscillation amplitude or even the start up condition. The optimum choice of inductance would be the one that places the oscillator at the verge of inductance limited regime (also called as current limited regime) and voltage limited regime. For a given bias current, phase noise would increase with inductance L, resulting in wastage of area. Similarly for a given bias current, placing the oscillator in voltage limited regime would result in increase in phase noise corresponding to wastage of power. The appropriate choice would be to choose a minimum inductance that would satisfy the minimum desired voltage swing for a given current. In this design, we have chosen the bias current to be 1.5 mA for each LC core.

From (4.4), we infer that the negative transconductance provided by the cross coupled devices must be greater than 3 mS. This is achieved by using NMOS and PMOS cross-coupled pairs as already mentioned. The size of PMOS and NMOS switching devices is

decided by taking into account the additional bias current provided by the coupling devices $M_{3a} - M_{3b}$ for PMOS, which should satisfy the relation (4.4) and also assure the symmetric ISF for the oscillator. The transconductance of $M_{3a} - M_{3b}$ must be such that the loop gain from drain of M_{b2}, M_{3b}, M_{b3}, M_{3a} and back to the drain of M_{b2} must be less than one. If it exceeds one, then oscillations at v_{s1} and v_{s2} would result in AM modulated output waveform [16]. The transistors are designed taking this loop gain into account. Minimum length devices are chosen to keep the parasitics low, and the switching transistors are appropriately fingered to minimize the noise due to gate resistance. The aspect ratio for the devices in Fig 3.2 are summarized in Table 4.1.

Table 4.1. Device aspect ratio of Fig. 3.2.

Transistors	**Aspect Ratio**
$M_{1a} - M_{1b}$	$4\ X\ 2.25\ \mu m/0.18\ \mu m$
$M_{2a} - M_{2b}$	$8\ X\ 3.50\ \mu m/0.18\ \mu m$
$M_{3a} - M_{3b}$	$10\ X\ 2.9\ \mu m/0.18\ \mu m$
$M_{b1} - M_{b3}$	$12\ X\ 6.0\ \mu m/0.5\ \mu m$

The simulated tuning curve of the proposed QVCO is shown in Fig. 4.7. Buffers are designed in common source configuration to tap the signals out of the LC tanks. For testing purposes, the buffers are designed to drive 50 Ω load (cable impedance), hence huge amount of current has been burnt to keep the gain close to unity.

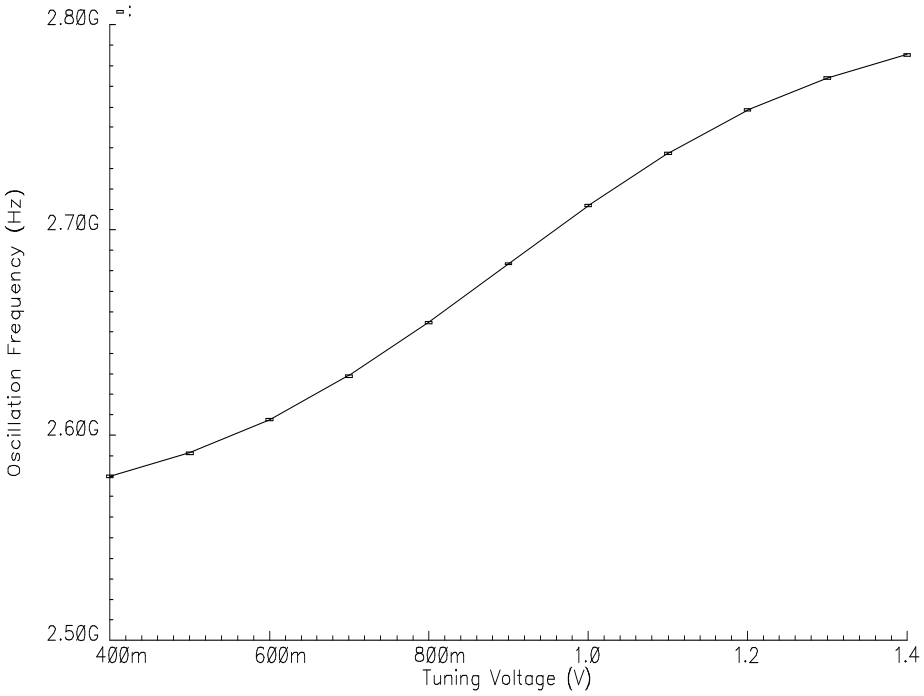

Fig. 4.7. Tuning curve of the proposed QVCO.

CHAPTER V

POST LAYOUT SIMULATION RESULTS

Careful layout techniques enhance the performance of the QVCO during post layout simulations. The layout of the QVCO has been made as symmetric as possible to cancel out the even harmonic oscillations at the output nodes. The ASSURA extractor captures the parasitic resistors and capacitors to the substrate that ensures precise post layout simulation results close to reality.

The inductors are placed far away from each other to minimize the mutual coupling between them, which would otherwise result in phase error. However, this is done at the cost of increased losses and parasitic capacitances [17]. The technology offers us a choice of 6 metal layers. Top thick metal layer offers low resistivity and it has been used to interconnect the oscillator core and inductor in each VCOs to prevent degradation of tank quality factor.

RF transistors that are equipped with guard ring and shield to prevent coupling between one another is used in the layout. The complete layout of the proposed QVCO is shown in Fig. 5.1.

The total layout area of the QVCO including the pads is 1.41 mm^2 ($1474\ \mu m\ X\ 959\ \mu m$).

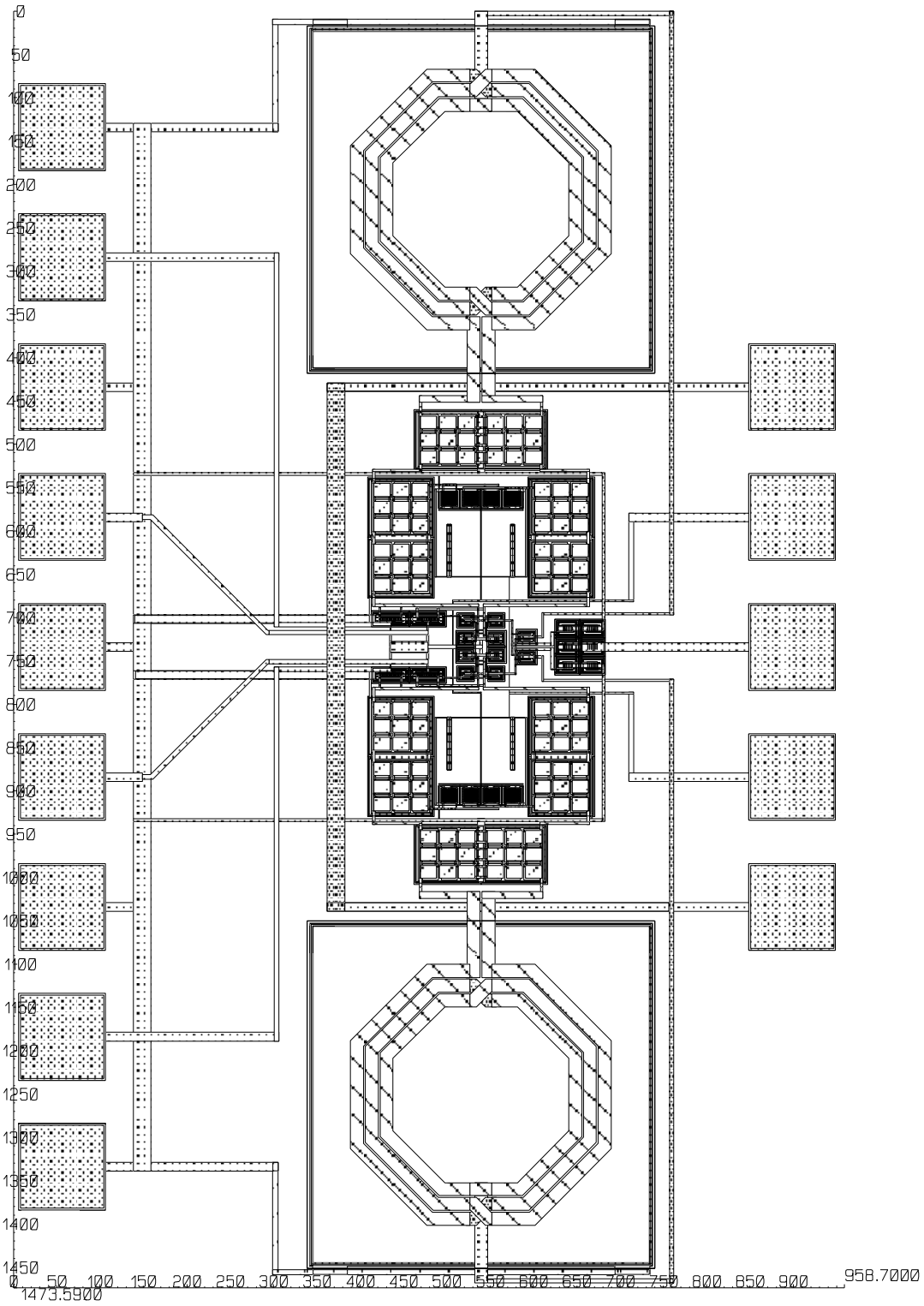

Fig. 5.1. Layout of the proposed QVCO.

The tuning curve of the QVCO from post layout simulation is shown in Fig 5.2 and the sensitivity of the QVCO has been observed to be 240 MHz/V.

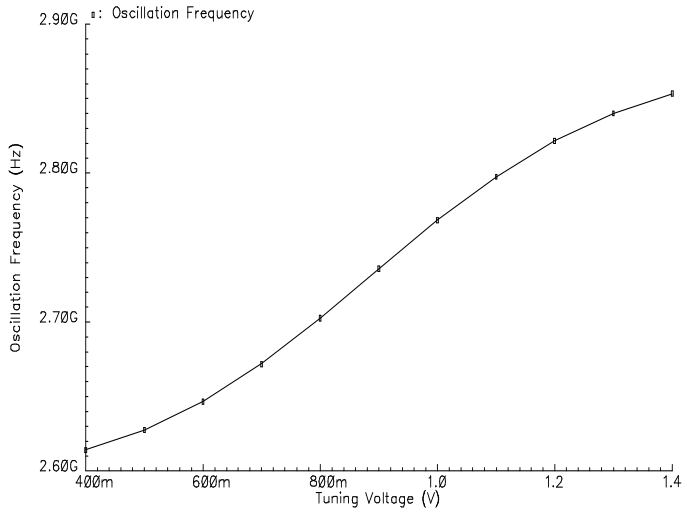

Fig. 5.2. Tuning characteristic of the proposed QVCO.

The phase noise (at 1 MHz offset) of the QVCO from post layout simulation is shown in Fig. 5.3.

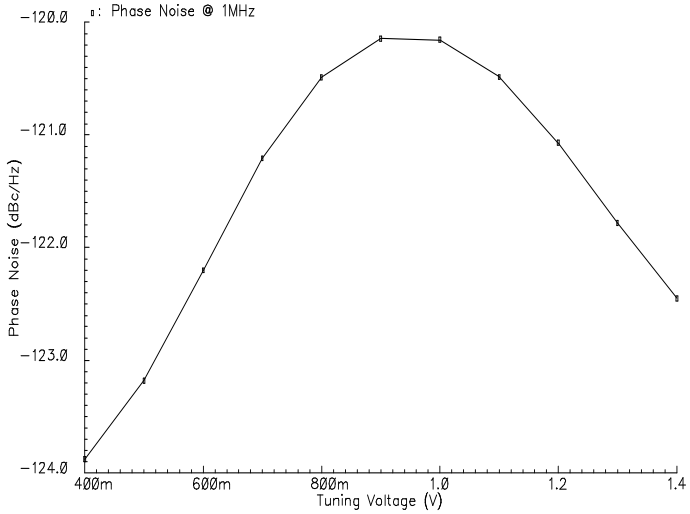

Fig. 5.3. Phase noise of QVCO.

Table 5.1 summarizes the simulation results of the proposed QVCO in typical corner.

Table 5.1. Performance summary.

Parameter	Value	Units
Tuning Range	2.61-2.85	GHz
Worst Case Phase Noise (@1MHz)	-120.4	dBc/Hz
Sensitivity (K_{VCO})	240	MHz/V
Power Supply	1.8	V
Current Consumption	3.0	mA
Area	1.41	mm^2

The figure of merit (FOM) for the oscillator is defined as,

$$FOM = 10\log\left(\left(\frac{f_0}{f_m}\right)^2\left(\frac{1}{\mathcal{L}(f_m)P}\right)\right) \text{ dBc/Hz}$$

where f_o is the oscillation frequency, f_m is the offset frequency, $\mathcal{L}(f_m)$ is phase noise at offset f_m and P is power dissipation in mW. The FOM for the proposed oscillator is found to be 181.7. Performance of the proposed VCO across process corners is summarized in Table 5.2. H and L represent fast and slow corners of MIMCAPs, induct-

Table 5.2. Phase noise (at 1 MHz offset) across corners.

	Phase Noise at 1 MHz (dBc/Hz)					
Tuning Voltage	**0.4 V**	**0.6 V**	**0.8 V**	**1.0 V**	**1.2 V**	**1.4 V**
FFH	-122.141	-121.583	-119.694	-118.935	-119.238	-119.417
SSL	-118.343	-119.322	-119.471	-120.258	-121.954	-123.325
FSH	-123.867	-122.169	-120.197	-119.566	-120.308	-121.564
SFH	-122.977	-121.405	-119.785	-119.706	-120.914	-122.081
FFL	-123.192	-121.910	-120.491	-120.074	-121.074	-121.820
SSH	-122.374	-121.135	-119.712	-119.804	-121.154	-122.307
FSL	-122.589	-121.617	-120.461	-120.540	-121.683	-122.743
SFL	-119.907	-119.398	-118.800	-119.228	-120.345	-120.900

-ors and MOS varactors. The tuning range of the QVCO across corners is summarized in Table 5.3. H and L represent fast and slow corners of MIMCAPs and inductors.

Table 5.3. Tuning range across corners.

Corner	Oscillating Frequency (GHz)	Tuning range (MHz)
TTT	2.61-2.85	240
FFH	2.83-3.08	250
SSL	2.42-2.65	230
FSH	2.83-3.08	250
SFH	2.83-3.08	250
FFL	2.45-2.68	230
SSH	2.80-3.05	250
FSL	2.42-2.65	230
SFL	2.42-2.65	230

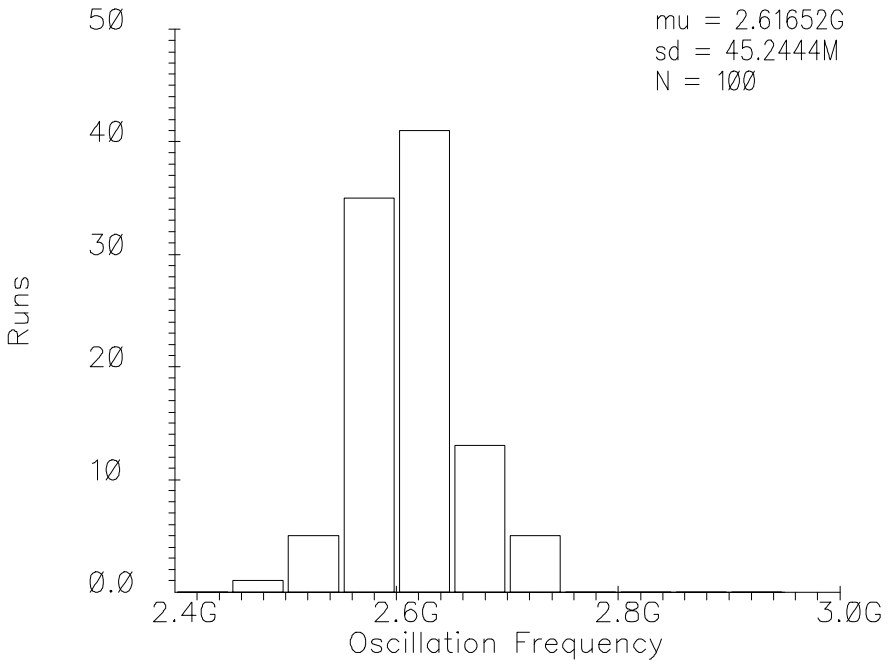

Fig. 5.4. Monte Carlo simulation result for V_{tune} = 0.4 V.

Monte Carlo simulations were performed to predict the variation in the oscillation frequency across corners. Parameters defining MOS transistors and MIMCAPs were varied in Gaussian distribution manner in Monte Carlo simulations. Fig. 5.4 and Fig. 5.5 show the Monte Carlo results for the lowest and the highest oscillation frequency.

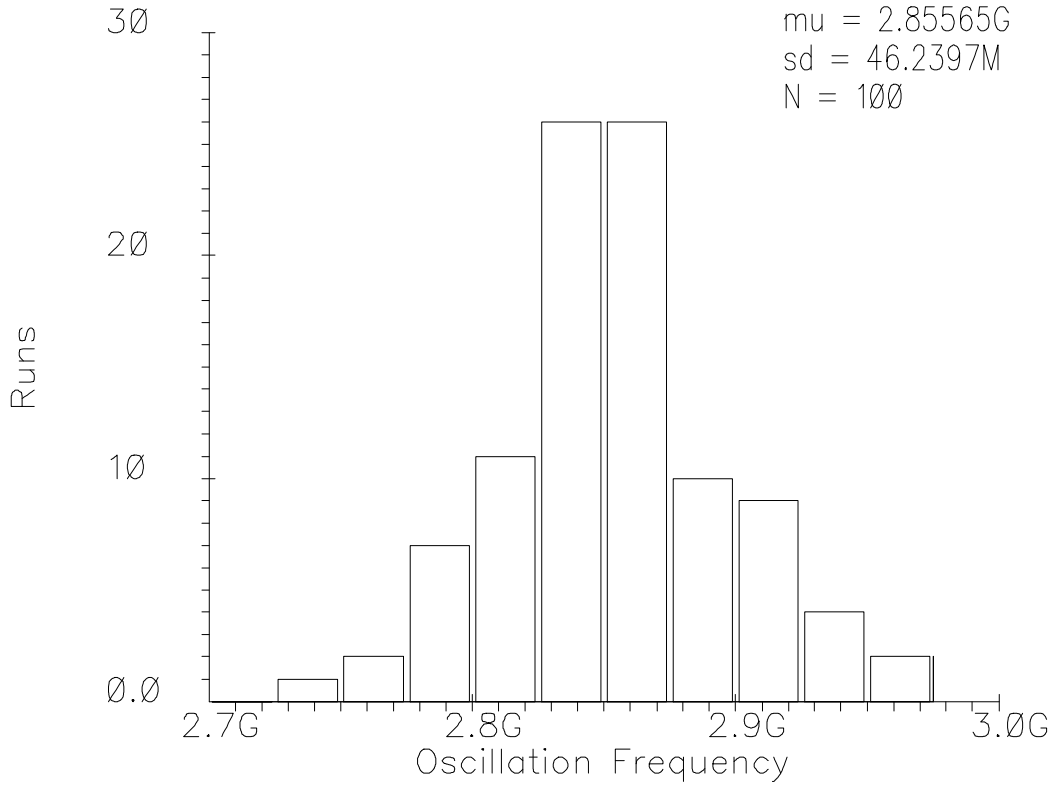

Fig. 5.5. Monte Carlo simulation result for V_{tune} = 1.4 V.

From Fig 5.4 we observe that the lowest oscillation frequency for V_{tune} = 400 mV across corners is 2.45 GHz. Similar observation from Fig. 5.5 reveals that the highest frequency for V_{tune} = 1.4 V across corners is 2.98 GHz. Comparing this with the results tabulated in Table 5.2 we can conclude that the most sensitive device causing the variation in the oscillation frequency across corners is the MIMCAPs. Since inductors

are generally huge in size, oscillation frequency is insensitive to variations in them across corners as it is evident from Monte Carlo results which take into account only MIMCAPs and MOS transistors. When oscillators are used in RF system such variations in the oscillation frequency must be taken into account during the design.

The performance of the proposed QVCO has been compared with other reported works in Table 5.4. It can be observed that the current recycling mechanism has enabled lower power consumption compared to others, while retaining better phase noise.

Table 5.4. Performance comparison.

Refere -nce	**Process**	F_0 **(GHz)**	**Frequency Range (GHz)**	**Q**	**Phase Noise (dBc/Hz)**	**Power (mW**	V_{DD} **(V)**	**FOM**
[5]	0.35 µm	1.82	1.67-1.97	6	-140@3M	50	2	178
[18]	0.18 µm	2.00	1.90-2.10	NA	-119@1M	11	1.1	175
[19]	0.25 µm	1.57	1.36-1.69	20	-133.5@600K	30	2	181
[20]	0.18 µm	1.10	1.04-1.39	NA	-120@1M	5.4	1.8	174
[21]	0.13 µm	2.18	0.75-2.20	NA	-120@1M	28.8	1.2	172
This Work	0.18 µm	2.70	2.61-2.85	12	-120@1M	5.4	1.8	182

.

CHAPTER VI

CONCLUSION

In this thesis, a new coupling mechanism is investigated to implement a quadrature voltage controlled oscillator with minimum power consumption and better phase noise. The proposed coupling mechanism saves power by recycling its bias current back into the LC tank (as explained in Chapter III) such that the power consumed by the coupling network is negligible.

It is observed that the coupled LC VCOs tend to have more than one possible modes of operation. So, mathematical analysis is done to analyze the stable mode of operation for this QVCO and other performance analysis has been done to compare the proposed QVCO with the conventional design. The proposed architecture provides higher amplitude for the same power consumption compared to other conventional designs and hence ensures better phase noise.

The proposed QVCO is designed in TSMC 0.18 μm technology. The QVCO achieved a worst case phase noise of -120 dBc/Hz at 1 MHz offset and consumed only 3 mA current from 1.8 V supply. Compared to other conventional QVCOs the proposed QVCO exhibits better phase noise and power efficiency.

REFERENCES

[1] A. Rofougaran, J. Rael, M. Rofougaran, A. Abidi, "A 900MHz CMOS LC-Oscillator with Quadrature Outputs," *IEEE ISSCC Dig. Tech. Papers*, Feb. 1996, pp. 392-393.

[2] A. Mirzaei, M. E. Heidari, R. Bagheri, S. Chehrazi and A. A.Abidi, "The Quadratutre LC Oscillator: A Complete Portrait Based on Injection Locking," *IEEE J. Solid-State Circuits,* vol. 42, no. 9, pp. 1916-1932, Sep. 2007.

[3] S. L. J. Gierkink, S. Levantino, R. C. Fyre, C. Samori, and V. Boccuzzi, "A Low-Phase Noise 5-GHz CMOS Quadrature VCO Using Superharmonic Coupling," *IEEE J. Solid-State Circuits,* vol. 38, no. 7, pp. 1148-1154, July 2003.

[4] A. Hajimiri, T. Lee, "Design Issues in CMOS Differential LC Oscillators," *IEEE J. Solid-State Circuits,* vol. 34, n0. 5, pp. 717-724, May 1999.

[5] P. Andreani, A. Bonfanti, L. Romano and C. Samori, "Analysis and Design of 1.8GHz CMOS LC Quadrature VCO," *IEEE J. Solid-State Circuits*, vol. 37, no. 12, pp. 1737-1747, Dec. 2002.

[6] A. Mirzaei and M. E. Heidari, "On the Mode Analysis of Coupled Oscillators," *IEEE International Midwest Symposium on Circuits and Systems,* pp. 819-822, Sept. 2009.

[7] J. Groszkowski, "The Interdependence of Frequency Variation and

Harmonic Content, and the Problem of Constant-Frequency Oscillators," *Proc. Institute of Radio Engineers,"* vol. 21, July 1933, pp. 958-981.

[8] P. Tortori, D. Guermandi, E. Franchi and A. Gnudi, "Quadrature VCO Based on Direct Second Harmonic Locking," *Proc. IEEE Int. Symp. Circuits and Systems (ISCAS),* vol. 1, Sept. 2004, pp. I-169 - I-172.

[9] T. Lee, *Design of Radio-Frequency Integrated Circuits*, 2nd ed., Cambridge UK: Cambridge University Press, 1998.

[10] C. W. Yao and A. N. Willson Jr., "Energy-Circulation Quadrature LC VCO," *Proc. IEEE Int. Symp. on Circuits and Systems (ISCAS),* Sept. 2006, pp. 4006-4009.

[11] M. Danesh and J. R. Long, "Differentially Driven Symmetric Microstrip Inductors," *IEEE Trans. Microwave Theory and Techniques,* vol. 50, pp. 332-341, Jan. 2002.

[12] T. H. Lee and A. Hajimiri, "Oscillator Phase Noise: A Tutorial," *IEEE J. Solid-State Circuits,* vol. 35, no. 3, pp. 326-336, March 2000.

[13] P. Andreani and S. Mattisson, "On the use of MOS Varactors for RF VCO's," *IEEE J. Solid-State Circuits,* vol. 35, no. 6, pp. 905-910, June 2000.

[14] E. Hegazi, A. Abidi, "Varactor Characteristics, Oscillator Tuning Curves, and AM-FM Conversion," *IEEE J. Solid-State Circuits,* vol. 38, no. 6, pp. 1033-1039, June 2003.

[15] D. Ham and A. Hajimiri, "Concepts and Methods in Optimization of Integrated LC VCOs," *IEEE J. Solid-State Circuits,* vol. 36, no. 6, pp. 1-6, June 2001.

[16] T. M. Hancock and G. M. Rebeiz, "A Novel Superharmonic Coupling Topology for Quadrature Oscillator Design at 6 GHz," *IEEE Radio Frequency Integrated Circuits (RFIC) Symp. Dig. Papers,* pp. 285-288, June 2004.

[17] P. Andreani and X. Wang, "On the Phase-Noise and Phase-Error Performances of Multiphase CMOS LC VCOs," *IEEE J. Solid-State Circuits,* vol. 39, no. 11, pp. 1883-1393, Nov. 2004.

[18] P. Upadhyaya, D. Heo, D. M. Rector, Y. E. Chen, "A 1.1V Low Phase Noise CMOS Quadrature LC VCO with 4-way Center-tapped Inductor," *Proc. IEEE Microwave Symposium,* June 2007, pp. 847-850.

[19] P. Vancorenland and M. S. J. Steyaert, "A 1.57-GHz Fully Integrated Very Low-Phase-Noise Quadrature VCO," *IEEE J. Solid-State Circuits,* vol. 37, no. 5, pp. 653-656, May 2002.

[20] H. R. Kim, S. M. Oh, S. D. Kim, Y. S. Youn and S. G. Lee, "Low Power Quadrature VCO with the Back-gate Coupling," *Proc. European Solid-State Circuits Conference,* Sept. 2003, pp. 699-701.

[21] D. Guermandi, P. Tortori, E. Franchi and A. Gnudi, "A 0.75 to 2.2GHz Continuously Tunable Quadrature VCO," *IEEE ISSCC Dig. Tech. Papers,* Feb. 2005, pp 536-615.

APPENDIX

Assuming that the cross-coupled differential pairs completely steer current from one arm to the other at the zero crossings of the output waveform, the differential equation obtained from Kirchhoff's law applied at the nodes I^+ and I^- (of Fig. 3.2) is given by,

$$C\frac{d^2V_{out}}{dt^2}+\frac{1}{R}\frac{dV_{out}}{dt}+\frac{V_{out}}{L}=\frac{d}{dt}[\mathrm{sgn}(V_{out}(t))I_t(t)] \tag{A.1}$$

where the tail current I_t is given by the summation of the bias current (I_{b0}) and the current injected at $2\omega_0(I_{inj})$ from one LC core to the other by the coupling devices acting on v_{s1} and v_{s2} (see Fig. 3.2).

The quadrature LC oscillator under injection at node I^+ (of Fig. 3.2) is modeled as shown in Fig. A.1. Similar modeling can be done at node I^- as well. Here $V_{out}(t) = V_{outI^+}(t) - V_{outI}^-(t)$.

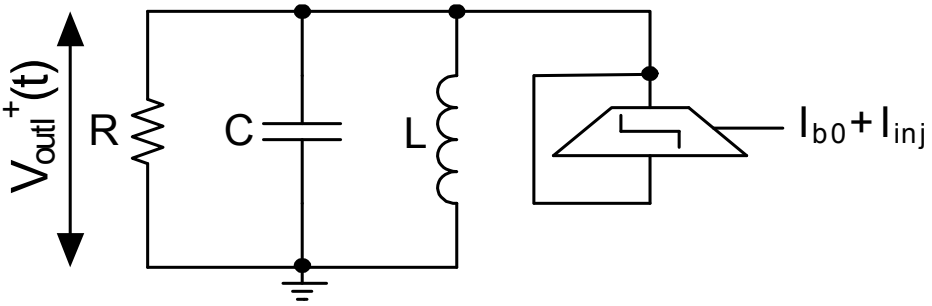

Fig. A.1. Modeling of LC oscillator under injection.

$$I_t(t) = I_{bo} + I_{inj}\cos(2\omega t + \theta_{inj}) \tag{A.2}$$

$$\frac{d}{dt}[\text{sgn}(V_{out}(t))I_t] = I_t\frac{d}{dt}\big(\text{sgn}(V_{out}(t))\big) + \text{sgn}(V_{out}(t))\frac{d}{dt}(I_t) \tag{A.3}$$

$$\frac{d}{dt}\big[\text{sgn}\big(V_{out}(t)\big)I_t\big] = I_t\left[\frac{d}{dV_{out}}\big(\text{sgn}(V_{out}(t))\big)\frac{dV_{out}}{dt}\right] + \text{sgn}(V_{out}(t))\frac{d}{dt}(I_t) \tag{A.4}$$

Assuming the solution for $V_{out}(t)$ to be of the form,

$$V_{out}(t) = V_a\cos(\omega t + \theta_{out}) \tag{A.5}$$

Taking the first two non zero coefficients in the Fourier series expansion of $\text{sgn}(V_{out}(t))$,

$$\text{sgn}(V_{out}(t)) = \frac{4}{\pi}\cos(\omega t + \theta_{out}) - \frac{4}{3\pi}\cos\big(3(\omega t + \theta_{out})\big) \tag{A.6}$$

Differentiating $\text{sgn}\big(V_{out}(t)\big)$ with respect to $V_{out}(t)$,

$$\frac{d}{dV_{out}(t)}\big[\text{sgn}\big(V_{out}(t)\big)\big] = \frac{d}{d(V_a\cos(\omega t + \theta_{out}))}\left[\frac{4}{\pi}\cos(\omega t + \theta_{out}) - \frac{4}{3\pi}\cos\big(3(\omega t + \theta_{out})\big)\right] \tag{A.7}$$

$$\Rightarrow \frac{1}{V_a}\frac{d}{d(\cos(\omega t + \theta_{out}))}\left[\frac{4}{\pi}\cos(\omega t + \theta_{out}) - \frac{16}{3\pi}\cos^3(\omega t + \theta_{out}) + \frac{4}{\pi}\cos(\omega t + \theta_{out})\right] \tag{A.8}$$

$$\Rightarrow \frac{1}{V_a}\left[\frac{8}{\pi} - \frac{16}{\pi}\cos^2(\omega t + \theta_{out})\right] \tag{A.9}$$

$$\frac{d}{dV_{out}(t)}\big[\text{sgn}\big(V_{out}(t)\big)\big] = -\frac{1}{V_a}\frac{8}{\pi}\cos\big(2(\omega t + \theta_{out})\big) \tag{A.10}$$

From (A.2) and (A.10),

$$I_t(t)\frac{d}{dV_{out}(t)}\left[\text{sgn}\left(V_{out}(t)\right)\right] = \left[I_{b0} + I_{inj}\cos\left(2\omega t + \theta_{inj}\right)\right]\left[-\frac{1}{V_a}\frac{8}{\pi}\cos\left(2(\omega t + \theta_{out})\right)\right] \tag{A.11}$$

$$I_t(t)\frac{d}{dt}\left[\text{sgn}\left(V_{out}(t)\right)\right] = I_t(t)\frac{d}{dV_{out}(t)}\left[\text{sgn}\left(V_{out}(t)\right)\right][-V_a\omega\sin(\omega t + \theta_{out})] \tag{A.12}$$

$$\Rightarrow \left[I_{b0} + I_{inj}\cos\left(2\omega t + \theta_{inj}\right)\right]\left[\frac{8}{\pi}\cos\left(2(\omega t + \theta_{out})\right)\right][\omega\sin(\omega t + \theta_{out})] \tag{A.13}$$

Expanding (A.13), we have

$$I_t(t)\frac{d}{dt}\left[\text{sgn}\left(V_{out}(t)\right)\right] = I_t(t)\left[\frac{4}{\pi}\omega sin\left(3(\omega t + \theta_{out})\right) - \frac{4}{\pi}\omega\sin(\omega t + \theta_{out})\right] \tag{A.14}$$

Substituting for $I_t(t)$ and expanding (A.14) we get,

$$I_t(t)\frac{d}{dt}\left[\text{sgn}\left(V_{out}(t)\right)\right] = \frac{4}{\pi}I_{b0}\omega\sin\left(3(\omega t + \theta_{out})\right) - \frac{4}{\pi}I_{b0}\omega\sin(\omega t + \theta_{out}) + \frac{4}{\pi}I_{inj}\omega\sin\left(3(\omega t + \theta)\right)\cos\left(2\omega t + \theta_{inj}\right) - \frac{4}{\pi}I_{inj}\omega\sin(\omega t + \theta_{out})\cos\left(2\omega t + \theta_{inj}\right) \tag{A.15}$$

$$\Rightarrow \frac{4}{\pi}\Big(\sin\big(3(\omega t+\theta_{out})\big)-\sin(\omega t+\theta_{out})\Big)I_{b0}\omega$$
$$+\frac{2}{\pi}I_{inj}\omega\sin\big(5\omega t+3\theta_{out}+\theta_{inj}\big)$$
$$+\frac{2}{\pi}I_{inj}\omega\sin\big(\omega+3\theta_{out}-\theta_{inj}\big)-\frac{2}{\pi}I_{inj}\omega\sin\big(3\omega t+\theta_{out}+\theta_{inj}\big) \quad (A.16)$$
$$+\frac{2}{\pi}I_{inj}\omega\sin\big(\omega t+\theta_{inj}-\theta_{out}\big)$$

Using (A.6),

$$\operatorname{sgn}\big(V_{out}(t)\big)\frac{d}{dt}I_t(t)= \quad (A.17)$$
$$\left[\frac{4}{\pi}\cos(\omega t+\theta_{out})-\frac{4}{3\pi}\cos\big(3(\omega t+\theta_{out})\big)\right]\frac{d}{dt}I_t(t)$$

$$\Rightarrow\left[\frac{4}{\pi}\cos(\omega t+\theta_{out})-\frac{4}{3\pi}\cos\big(3(\omega t+\theta_{out})\big)\right]\left[-2I_{inj}\omega\sin\big(2\omega t+\theta_{inj}\big)\right] \quad (A.18)$$

$$\Rightarrow -\frac{4}{\pi}I_{inj}\omega\sin\big(3\omega t+\theta_{out}+\theta_{inj}\big)-\frac{4}{\pi}I_{inj}\omega\sin\big(\omega t+\theta_{inj}-\theta_{out}\big) \quad (A.19)$$
$$+\frac{4}{3\pi}I_{inj}\omega\sin\big(5\omega t+3\theta_{out}+\theta_{inj}\big)-\frac{4}{3\pi}\,I_{inj}\omega\sin\big(\omega t+3\theta_{out}-\theta_{inj}\big)$$

Using (A.16) and (A.19) in (A.3),

$$\frac{d}{dt}[\operatorname{sgn}(V_{out}(t))I_t]=\frac{4}{\pi}I_{b0}\omega\sin\big(3(\omega t+\theta_{out})\big)-\frac{4}{\pi}I_{b0}\omega\sin(\omega t+\theta_{out})$$
$$+\frac{10}{3\pi}I_{inj}\omega\sin\big(5\omega t+3\theta_{out}+\theta_{inj}\big)+\frac{2}{3\pi}I_{inj}\omega\sin(\omega t+3\theta_{out}-\theta_{inj}) \quad (A.20)$$
$$-\frac{6}{\pi}I_{inj}\omega\sin\big(3\omega t+\theta_{out}+\theta_{inj}\big)-\frac{2}{\pi}I_{inj}\omega\sin(\omega t+\theta_{inj}-\theta_{out})$$

Using $V_{out} = V_a \cos(\omega t + \theta_{out})$,

$$C\frac{d^2V_{out}}{dt^2} + \frac{1}{R}\frac{dV_{out}}{dt} + \frac{V_{out}}{L} = \\ -CV_a\omega^2\cos(\omega t + \theta_{out}) - \frac{\omega}{R}V_a\sin(\omega t + \theta_{out}) + \frac{1}{L}V_a\cos(\omega t + \theta_{out}) \tag{A.21}$$

After the steady state is achieved, it can be assumed that the oscillating frequency is decided by the inductance L and capacitance C of the tank,

$$\omega = \omega_0 = \frac{1}{\sqrt{LC}} \tag{A.22}$$

Hence (A.21) can be written as,

$$C\frac{d^2V_{out}}{dt^2} + \frac{1}{R}\frac{dV_{out}}{dt} + \frac{V_{out}}{L} = -\frac{\omega_0}{R}V_a\sin(\omega t + \theta_{out}) \tag{A.23}$$

From (A.1), (A.20) and (A.23) (assuming $\omega = \omega_0$),

$$\frac{V_a}{R}\sin(\omega_0 t + \theta_{out}) = \frac{4}{\pi}I_{b0}\sin(\omega_0 t + \theta_{out}) - \frac{4}{\pi}I_{b0}\sin(3(\omega_0 t + \theta_{out})) \\ -\frac{10}{3\pi}I_{inj}\omega\sin(5\omega t + 3\theta_{out} + \theta_{inj}) - \frac{2}{3\pi}I_{inj}\omega\sin(\omega t + 3\theta_{out} - \theta_{inj}) \\ +\frac{6}{\pi}I_{inj}\omega\sin(3\omega t + \theta_{out} + \theta_{inj}) + \frac{2}{\pi}I_{inj}\omega\sin(\omega t + \theta_{inj} - \theta_{out}) \tag{A.24}$$

Equating the coefficients of the first harmonic (due to harmonic balance) in (A.24),

$$\frac{V_a}{R}\cos(\theta_{out}) = \frac{4}{\pi}I_{b0}\cos(\theta_{out}) + \frac{2}{\pi}I_{inj}\cos(\theta_{inj} - \theta_{out}) \\ -\frac{2}{3\pi}I_{inj}\cos(3\theta_{out} - \theta_{inj}) \tag{A.25}$$

Dividing (A.25) by $\cos(\theta_{out})$,

$$\frac{V_a}{R} = \frac{4}{\pi} I_{b0} + \frac{2}{\pi} I_{inj} \frac{\cos(\theta_{inj} - \theta_{out})}{\cos(\theta_{out})} - \frac{2}{3\pi} I_{inj} \frac{\cos(3\theta_{out} - \theta_{inj})}{\cos(\theta_{out})} \tag{A.26}$$

$$\begin{aligned} \frac{V_a}{R}\sin(\theta_{out}) = \frac{4}{\pi} I_{b0} \sin(\theta_{out}) + \frac{2}{\pi} I_{inj} \sin(\theta_{inj} - \theta_{out}) \\ - \frac{2}{3\pi} I_{inj} \sin(3\theta_{out} - \theta_{inj}) \end{aligned} \tag{A.27}$$

Dividing (A.27) by $\sin(\theta_{out})$,

$$\frac{V_a}{R} = \frac{4}{\pi} I_{b0} + \frac{2}{\pi} I_{inj} \frac{\sin(\theta_{inj} - \theta_{out})}{\sin(\theta_{out})} - \frac{2}{3\pi} I_{inj} \frac{\sin(3\theta_{out} - \theta_{inj})}{\sin(\theta_{out})} \tag{A.28}$$

From (A.26) and (A.28),

$$\begin{aligned} \frac{2}{\pi} I_{inj} \frac{\cos(\theta_{inj} - \theta_{out})}{\cos(\theta_{out})} - \frac{2}{3\pi} I_{inj} \frac{\cos(3\theta_{out} - \theta_{inj})}{\cos(\theta_{out})} = \\ \frac{2}{\pi} I_{inj} \frac{\sin(\theta_{inj} - \theta_{out})}{\sin(\theta_{out})} - \frac{2}{3\pi} I_{inj} \frac{\sin(3\theta_{out} - \theta_{inj})}{\sin(\theta_{out})} \end{aligned} \tag{A.29}$$

$$\begin{aligned} \frac{\cos(\theta_{inj} - \theta_{out})}{\cos(\theta_{out})} - \frac{1}{3} \frac{\cos(3\theta_{out} - \theta_{inj})}{\cos(\theta_{out})} = \\ \frac{\sin(\theta_{inj} - \theta_{out})}{\sin(\theta_{out})} - \frac{1}{3} \frac{\sin(3\theta_{out} - \theta_{inj})}{\sin(\theta_{out})} \end{aligned} \tag{A.30}$$

$$\tan(\theta_{out}) = \frac{\sin(\theta_{inj} - \theta_{out}) - \frac{1}{3}\sin(3\theta_{out} - \theta_{inj})}{\cos(\theta_{inj} - \theta_{out}) - \frac{1}{3}\cos(3\theta_{out} - \theta_{inj})} \tag{A.31}$$

$$\tan(\theta_{out}) = \frac{3\sin(\theta_{inj} - \theta_{out}) - \sin(3\theta_{out} - \theta_{inj})}{3\cos(\theta_{inj} - \theta_{out}) - \cos(3\theta_{out} - \theta_{inj})} \tag{A.32}$$

$$\tan(\theta_{out}) = \frac{2\sin(\theta_{inj} - \theta_{out}) + [\sin(\theta_{inj} - \theta_{out}) - \sin(3\theta_{out} - \theta_{inj})]}{2\cos(\theta_{inj} - \theta_{out}) + [\cos(\theta_{inj} - \theta_{out}) - \cos(3\theta_{out} - \theta_{inj})]} \tag{A.33}$$

Using trigonometric identity, (A.33) can be written as,

$$\tan(\theta_{out}) = \frac{\sin(\theta_{out})}{\cos(\theta_{out})} \Rightarrow \frac{\sin(\theta_{inj} - \theta_{out}) + \cos(\theta_{out})\sin(\theta_{inj} - 2\theta_{out})}{\cos(\theta_{inj} - \theta_{out}) - \sin(\theta_{out})\sin(\theta_{inj} - 2\theta_{out})} \tag{A.34}$$

$$\sin(\theta_{out})\left[\cos(\theta_{inj} - \theta_{out}) - \sin(\theta_{out})\sin(\theta_{inj} - 2\theta_{out})\right] = \cos(\theta_{out})\left[\sin(\theta_{inj} - \theta_{out}) + \cos(\theta_{out})\sin(\theta_{inj} - 2\theta_{out})\right] \tag{A.35}$$

Expanding (A.35) and simplifying,

$$2\sin(\theta_{out})\cos(\theta_{\mathrm{out}})\cos(\theta_{inj}) - \sin(\theta_{inj})\left[\cos^2(\theta_{out}) - \sin^2(\theta_{out})\right] - \sin(\theta_{inj})\cos(2\theta_{out}) + \cos(\theta_{inj})\sin(2\theta_{out}) = 0 \tag{A.36}$$

Simplifying (A.36) using trigonometric identities,

$$2\sin(2\theta_{out})\cos(\theta_{inj}) - 2\sin(\theta_{inj})\cos(2\theta_{out}) + \cos(\theta_{inj})\sin(2\theta_{out}) = 0 \tag{A.37}$$

$$\sin(2\theta_{out})\cos(\theta_{inj}) = \cos(\theta_{inj})\sin(2\theta_{out}) \tag{A.38}$$

$$\tan(2\theta_{out}) = \tan(\theta_{inj}) \tag{A.39}$$

From (A.39),

$$2\theta_{out} = \theta_{inj}\ (or)\ \theta_{inj} + \pi \tag{A.40}$$

Therefore,

$$\theta_{out} = \frac{\theta_{inj}}{2}\ (or)\ \theta_{out} = \frac{\theta_{inj}}{2} + \frac{\pi}{2} \tag{A.41}$$

If $\theta_{out} = \theta_{inj}/2$, from (A.26) or (A.28) we have,

$$V_a = R\left[\frac{4}{\pi}I_{b0} + \frac{2}{\pi}I_{inj} - \frac{2}{3\pi}I_{inj}\right] = R\left[\frac{4}{\pi}I_{b0} + \frac{4}{3\pi}I_{inj}\right] \tag{A.42}$$

$$V_a = \frac{4}{\pi}I_{b0}R\left[1 + \frac{m}{3}\right] \tag{A.43}$$

where m is the coupling factor defined as,

$$m = \frac{I_{inj}}{I_{b0}} \tag{A.44}$$

If $\theta_{out} = \theta_{inj}/2 + \pi/2$, from (A.26) or (A.28) we have,

$$V_a = R\left[\frac{4}{\pi}I_{b0} - \frac{2}{\pi}I_{inj} + \frac{2}{3\pi}I_{inj}\right] = R\left[\frac{4}{\pi}I_{b0} - \frac{4}{3\pi}I_{inj}\right] \tag{A.45}$$

$$V_a = \frac{4}{\pi}I_{b0}R\left[1 - \frac{m}{3}\right] \tag{A.46}$$

Among the two solutions (A.43) and (A.46), the mode with higher amplitude will sustain after the oscillations startup. As amplitude settling mechanism is nonlinear, the mode with higher amplitude will grow and settle to a steady state value while damping out the mode with smaller amplitude.

VITA

Shriram Kalusalingam received his Bachelor degree in electronics and communication engineering from the College of Engineering, Guindy, Anna University, Chennai, India in 2007. In the fall of 2007, he joined Analog & Mixed Signal Center, Department of Electrical Engineering, Texas A&M University to pursue his M.S. degree under the supervision of Dr. Aydin Karsilayan. From May 2008 to August 2008 he had an internship with Texas Instruments, Bangalore, India, where he worked on low power low area charge-pump PLL. He was also an engineering intern with Broadcom Corporation, CA from January 2010 to May 2010 where he worked on wideband buffers for RF Front-End. He received his M.S in electrical engineering from Texas A & M University in 2010. He can be reached through the Department of Electrical and Computer Engineering, c/o Dr. Karsilayan, Texas A&M University, College Station, Texas 77843-3128.